Supporting Information

Efficient Natural Gas Upgrade Using Metal−Organic Frameworks with Two Different-Sized Aromatic Ring-Confined Nanotraps

Shu-Yi Li[a], Ying-Ying Xue[a], Jia-Wen Wang[a], Hai-Peng Li[a], Jiao Lei[a], Hong-Juan Lv[a], Xianhui Bu[b,*], Peng Zhang[a], Ying Wang[a], Wen-Yu Yuan[a], Quan-Guo Zhai[a,*]

[a]Key Laboratory of Applied Surface and Colloid Chemistry, Ministry of Education, School of Chemistry & Chemical Engineering, Shaanxi Normal University, Xi'an, Shaanxi, 710062, China

[b]Department of Chemistry and Biochemistry, California State University, Long Beach, California, 90840, USA

*To whom correspondence should be addressed: xianhui.bu@csulb.edu; zhaiqg@snnu.edu.cn

General materials and methods

All chemicals including $Co(CH_3COO)_2 \cdot 4H_2O$, 2,5-pyridinedicarboxylic acid (2,5-PDC), 1,4-terephthalic acid (BDC), naphthalene-2,6-dicarboxylic acid (2,6-NDC), 2,4,6-tri(4-pyridinyl)-1-pyridine (TPP), 1,3,5-tris(4-pyridyl)benzene (TPB), N,N-dimethylacetamide (DMA), N,N-dimethylformide (DMF), 1,3-dimethyl-3,4,5,6-tetrahydro-2(1H)-pyrimidinone (DMPU), ethanol (EtOH) and 1,1,1,5,5,5-hexafluoro-2,4-pentanedione (HFP) were purchased commercially and used without further purification. The powder X-ray diffraction (PXRD) tests were carried out on a MiniFlex 600 X-ray diffractometer (Rigaku, Japan). Thermogravimetric analyses (TGA) were carried out on a HCT-1 thermal analyzer with a ramp rate of 2 °C min^{-1} up to 570 °C in a nitrogen atmosphere.

Synthesis of {[Co₃(μ₃-OH)][Co(PDC)₂]₃(TPB)₃}ₙ (SNNU-185). A mixture of $Co(CH_3COO)_2 \cdot 4H_2O$ (50 mg), 2,5-PDC (17 mg), TPB (31 mg), DMF (3.0 mL) and EtOH (1.0 mL) was sealed in a 20 mL vial and heated at 130 °C for 5 days. After slow cooling to room temperature, red hexagonal prism crystals (Figure S1) were isolated. Pure sample was obtained by filtering and washing the raw product with hot DMF.

Synthesis of {[Co₃(μ₃-OH)][Co(PDC)₂]₃(TPP)₃}ₙ (SNNU-186). A mixture of $Co(CH_3COO)_2 \cdot 4H_2O$ (100 mg), 2,5-PDC (34 mg), TPP (62 mg), DMF (6.0 mL), DMA (2.0 mL) was sealed in a 20 mL vial and heated at 130 °C for 3 days. Pure red hexagonal prism crystals were obtained after filtering the hot solution.

Scale-up synthesis of SNNU-186. A decagram scale synthesis of SNNU-186 was carried out under reflux conditions. $Co(CH_3COO)_2 \cdot 4H_2O$ (12.00 g), 2,5-PDC (4.08 g), TPP (7.44 g), DMF (400 mL) and DMA (200 mL) were mixed in a round-bottom flask and refluxed at 125 °C for 3 days. Purified SNNU-186 was collected by filtration. After dried under air environments, about 12.7 g SNNU-186 was obtained.

Synthesis of SNNU-26. SNNU-26-Co was synthesized according to the previous work.[1] A mixture of $CoCl_2 \cdot 6H_2O$ (95 mg), BDC (33 mg), TPP (62 mg), DMA (4 mL), DMPU (2 mL), and HFP (28 μL) was sealed in a 20 mL vial and heated at 130 °C for 3 days. After cooling to room-temperature, red crystals were obtained by filtering and washing with DMA.

Synthesis of SNNU-28. SNNU-28-Co was synthesized according to the previous work.[1] A mixture of $CoCl_2 \cdot 6H_2O$ (95 mg), 2,6-NDC (43 mg), TPP (62 mg), DMA (4 mL), DMPU (2 mL), and HFP (28 μL) was sealed in a 20 mL vial and heated at 130 °C for 3 days. After cooling to room-temperature, red crystals were obtained by filtering and washing with DMA.

Single Crystal X-ray Diffraction Data. Crystallographic data of SNNU-185 and SNNU-186 were obtained on the single crystal diffractometer with graphite-monochromated Mo Kα radiation (λ = 0.71073 Å) and analyzed using SHELXTL and Olex 2 software. All non-hydrogen atoms were refined isotropically. The

detailed crystallographic data and the structure refinement parameters of SNNU-185 and SNNU-186 are summarized in Table S2.

Single-Component Gas Sorption Experiments. Gas sorption isotherms were measured on a Micromeritics 3-Flex surface-area and pore-size analyzer up to 1 atm of gas pressure by the static volumetric method. All used gases were of 99.99% purity. Prior to sorption analysis, methanol-exchanged compounds (60−100 mg) were loaded into the sample tube and dried at 358 K for 12 h by using the "outgas" function of the surface area analyzer to remove solvent molecules. The gas sorption isotherms for C_3H_8, C_2H_6 and CH_4 were recorded at 273, 283 and 298 K, respectively. The measured sample was regenerated at room temperature under vacuum conditions of 1.0×10^{-4} mmHg for 10 min. Brunauer-Emmett-Teller (BET) surface areas and pore size distribution data were determined from the N_2 adsorption isotherms at 77 K in a liquid nitrogen bath. A Dewar flask was used to maintain a constant temperature in the bath throughout the duration of the experiment.

Absorption Enthalpy Calculations. To extract the coverage-dependent isosteric heat of adsorption, the data were modeled with a virial-type expression composed of parameters a_i and b_i that are independent of temperature:

$$\ln P = \ln N + \frac{1}{T}\sum_{i=0}^{m} a_i N^i + \sum_{i=0}^{n} b_i N^i$$

$$Q_{st} = -R\sum_{i=0}^{m} a_i N^i$$

where P is the pressure, N is the amount adsorbed (or uptake), T is the temperature, and N determine the number of terms required to adequately describe the isotherm. R is the universal gas constant. The coverage dependencies of Q_{st} are calculated by fitting the data at 273 K and 298 K in the pressure range from 0 to 1 bar.

Ideal Adsorbed Solution Theory (IAST) Selectivity Calculations. Ideal adsorbed solution theory (IAST) was used to predict binary mixture adsorption from experimental pure gas isotherms. To perform the integrations required by IAST, single-component isotherms should be fitted with an appropriate model. The Langmuir-Freundlich (LF) equation was found to give the best fit to the experimental pure gas isotherms of compounds SNNU-185/186. Based on the equation parameters of pure gas adsorption, the IAST model was used to investigate the separation of C_2H_6/CH_4 and C_3H_8/CH_4 at 298 K.

Dynamic Gas Breakthrough Experiments. Dynamic breakthrough experiments were carried out on a home-built dynamic gas breakthrough set-up with a temperature of 273 K or 298 K being controlled by a circulating water bath. Prior to the breakthrough experiments, the samples were activated at 358 K for 12 h under vacuum conditions. The column contained activated samples of 790 mg (SNNU-185) and 792 mg (SNNU-186), respectively. After the adsorption and separation in the through-column unit adsorption bed, the gas was then flowed into the gas chromatographic detection system (GC-9790 II, SHIMADZU) for detection and analysis.

After the breakthrough experiment, the sample was regenerated under vacuum conditions of -0.09 MPa for 50 min, and then with a helium flow (30 mL min^{-1}) for 30 min at room temperature. For the comparison experiment of dynamic gas breakthrough tests, prior to the breakthrough experiments, mixed 500 mg SNNU-26-Co and 500 mg SNNU-28-Co samples were activated at 358 K for 12 h under vacuum conditions. The column contained activated 794 mg samples (SNNU-26-Co + SNNU-28-Co) during the breakthrough experiments.

Expected energy consumption. Considering that no heating is required during regeneration process, it is assumed that the major energy consumption comes from the vacuum pumps to remove gases from the MOF adsorbents, so a PSA cycle is more suitable than a TSA cycle.[2] However, it is difficult to obtain accurate regeneration costs without simulating a PSA cycle, which can only be speculated. Therefore, after mainly taking the energy consumption from the vacuum pumps into account, the expected energy penalty was calculated using the following formula:

$$\text{Energy consumption} = P \text{ (kW)} \times t \text{ (h)}$$

where the P = power of vacuum pump (KW, 0.4 kW), t = time used in the regeneration process of breakthrough tests (h). As a result, in this work, the expected energy penalty was calculated to be 0.33 kWh.

Calculation method of CH$_4$ productivity. The CH$_4$ productivity is defined by the breakthrough amount of CH$_4$, which is calculated by integration of the breakthrough curves $f(t)$ during a period from t_1 to t_2 according the following equation:

$$q(CH_4) = \left(\frac{C_{CH_4} F \times \int_{t1}^{t2} f(t)dt)/22.4}{} \right.$$

where C is gas concentration percentage, F is feed gas flow rate, t is adsorption time per gram and $\int_{t1}^{t2} f(t)dt$ is the integral area of breakthrough curves $f(t)$ during a period from t_1 to t_2.

Grand Canonical Monte Carlo (GCMC) Simulations. GCMC simulation method was used to study the interaction sites and adsorption distribution. The simulation was performed using Material Studio 8.0. In the simulation process, the structure is rigid. After geometrically optimizing crystal structures with the forcite module, a 2 × 2 × 2 supercell was created as a simulation box. The cut-off radius for van der Waals interaction is set to 18.5 Å, and the Ewald method deals with long-range electrostatic interaction. Each simulation process is set to 1 × 10^7 steps to reach a stable state. The total pressure of the gas is set to 1 bar and the temperature to 298 K.
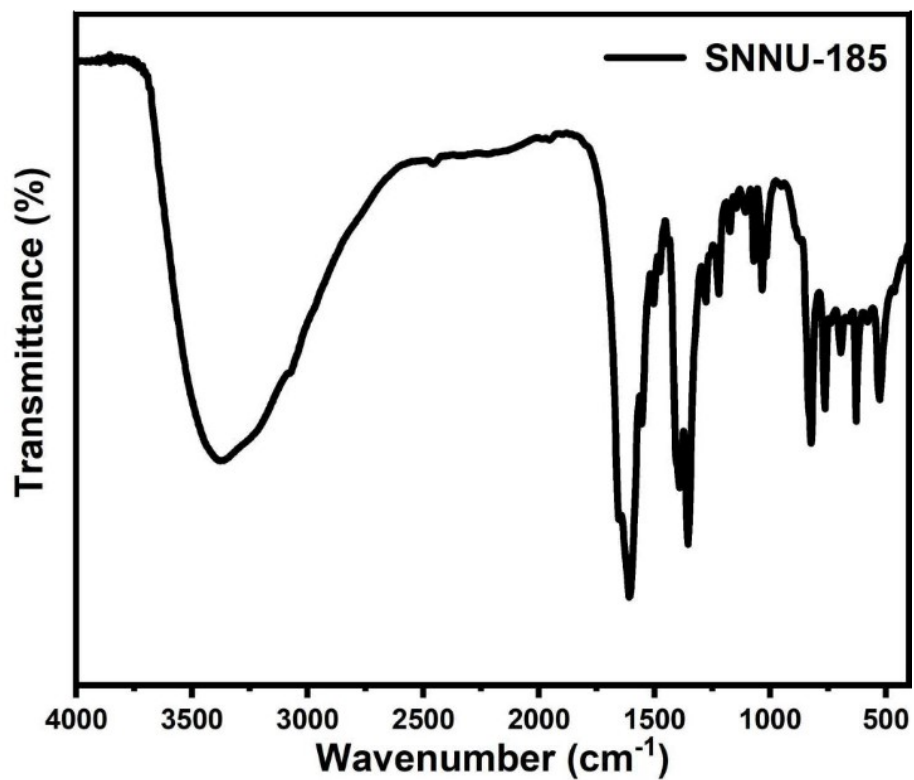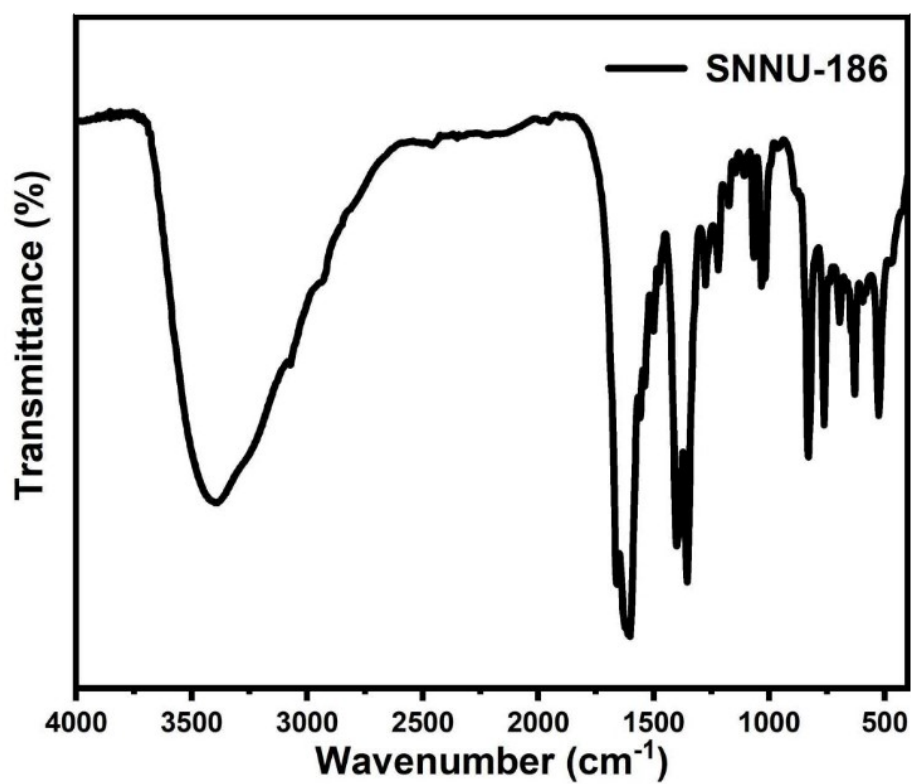
Results and Discussion
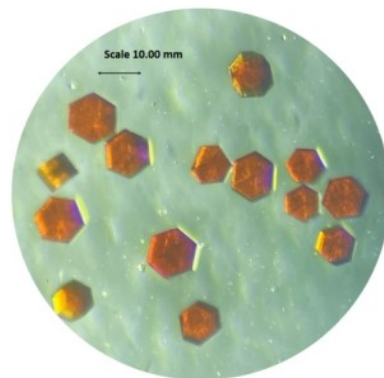
Figure S1. Photos of single crystals for SNNU-185 and SNNU-186.

Figure S2. FT-IR spectra of (a) SNNU-185 and (b) SNNU-186.
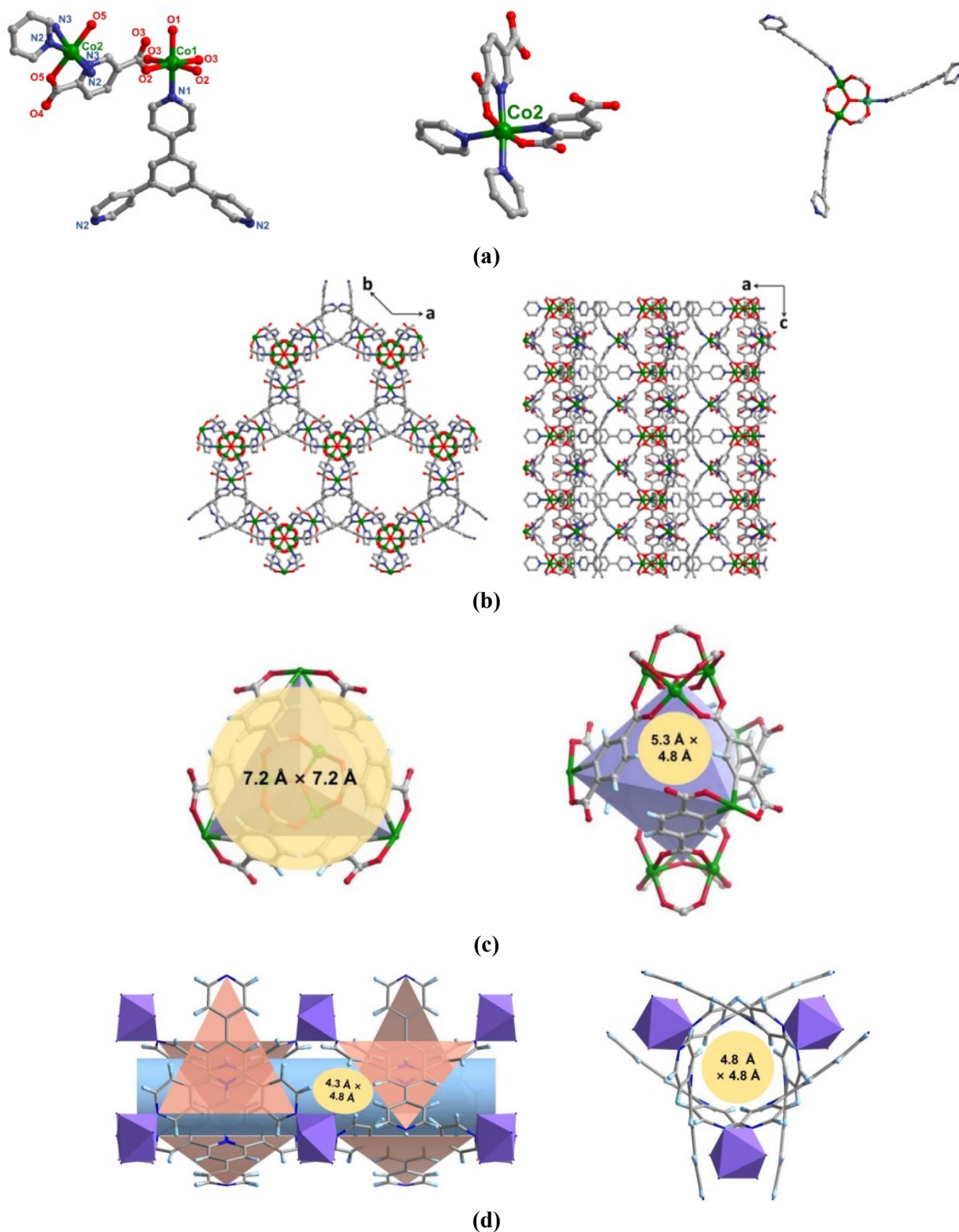
(a)

(b)

(c)

(d)

Figure S3. (a) Structural details of SNNU-185 which is isostructural with SNNU-54[3] (H atoms are omitted for clarity). (b) Detailed 3D structure of SNNU-185 (H atoms are omitted for clarity). (c) Structure of nanotrap 1: the available inner cavity is of ~7.2 Å × 7.2 Å (left) and the window size is of ~5.3 Å × 4.8 Å (right). This kind of large nanotraps is considered as C_3H_8-selective adsorption site. (d) Structure of nanotrap 2: the window size is of ~4.3 Å × 4.8 Å (left) and channel size is of ~4.8 Å × 4.8 Å (right). This kind of nanotraps is considered as C_2H_6-selective adsorption site.

(a)

(b)
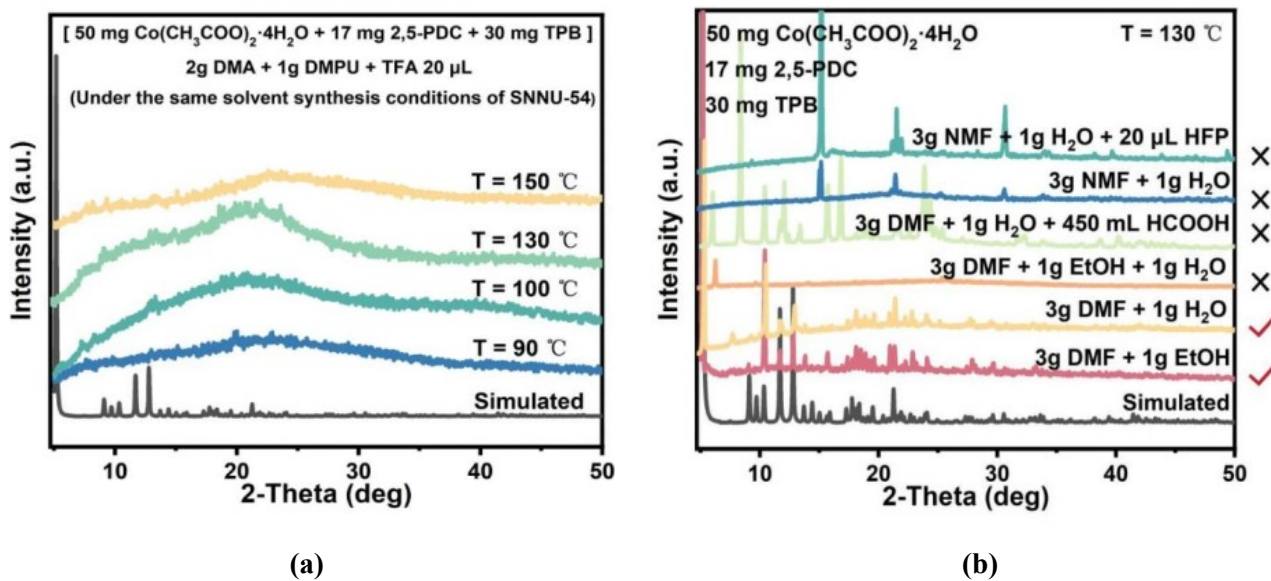
■ **Study process** of exploring the synthesis conditions of SNNU-185

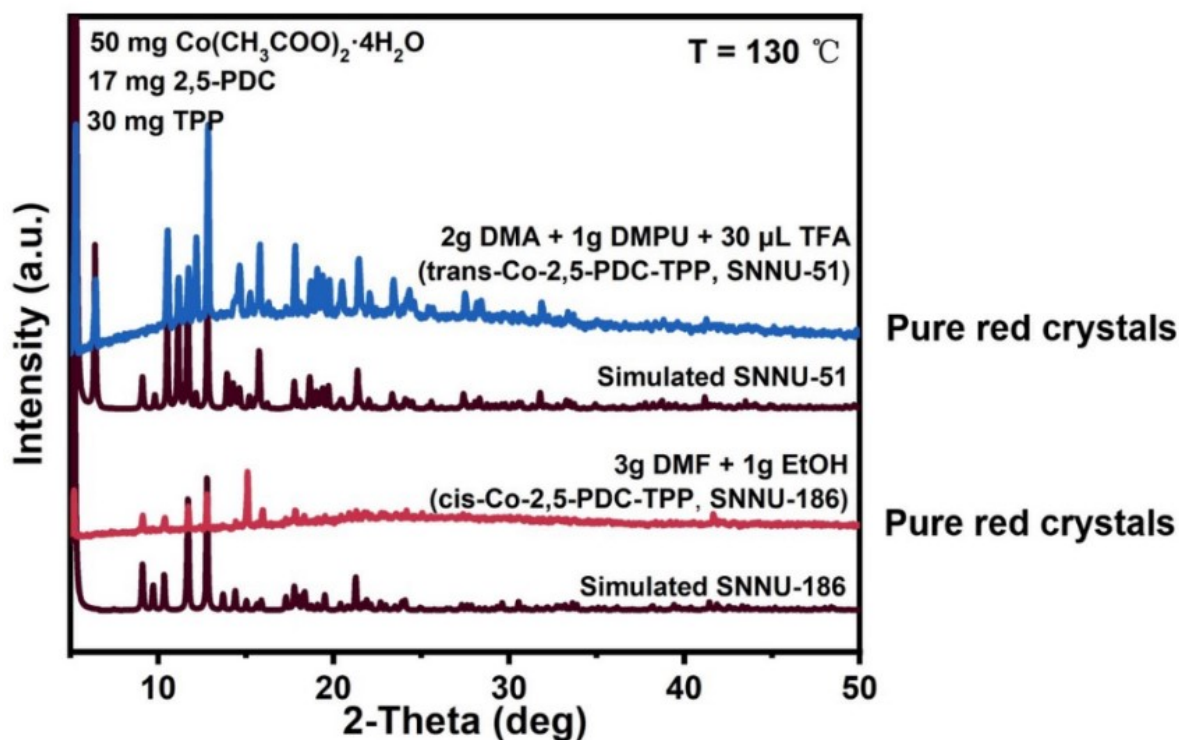1. Same solvents, same T as SNNU-54 → ✗ (Figure S4a, light green line)

2. Same solvents, different T → ✗ (Figure S4a)

3. Different solvents, same T → ✓ SNNU-185 (3g DMF + 1g EtOH, T = 130 ℃) (Figure S4b, red line)

(c)

Figure S4. Detailed study on exploring synthesis conditions of SNNU-185. (a) Partial PXRD patterns of the substance synthesized under the same solvent conditions of SNNU-54 and different temperature. (b) PXRD patterns of the substance synthesized under the different solvent conditions and 130℃ (SNNU-185 could be synthesized when 3g DMF and 1g EtOH were used as solvents). (c) Study process of exploring the synthesis conditions of SNNU-185 which can summarize the information of Figures S4a and S4b.

(a)

■ **Study process** of exploring the synthesis conditions of SNNU-186

1. Same solvents, same T as SNNU-54 → SNNU-51 (Pure crystals, Figure S5a, blue line)

2. Same solvents, same T as SNNU-185 → ✓ SNNU-186 (Pure crystals, Figure S5b, red line)

(b)

Figure S5. Detailed study on exploring synthesis conditions of SNNU-186. (a) PXRD patterns of SNNU-186 with cis-SBU and SNNU-51 with trans-SBU. (b) Study process of exploring the synthesis conditions of SNNU-186: as shown in the above figure (blue line), under the same synthesis conditions of SNNU-54 (2g DMA, 1g DMPU and 30 μL TFA), SNNU-186 could not be synthesized and the obtained MOF is SNNU-51 (trans-Co-2,5-PDC-TPP). Then, considering that SNNU-185 could be synthesized under the conditions of 3g DMF and 1g EtOH (T = 130 °C) (Figure S4), 3g DMF and 1g EtOH (T = 130 °C) were used as synthesis conditions to try to synthesize SNNU-186 and SNNU-186 (red line) was finally obtained.
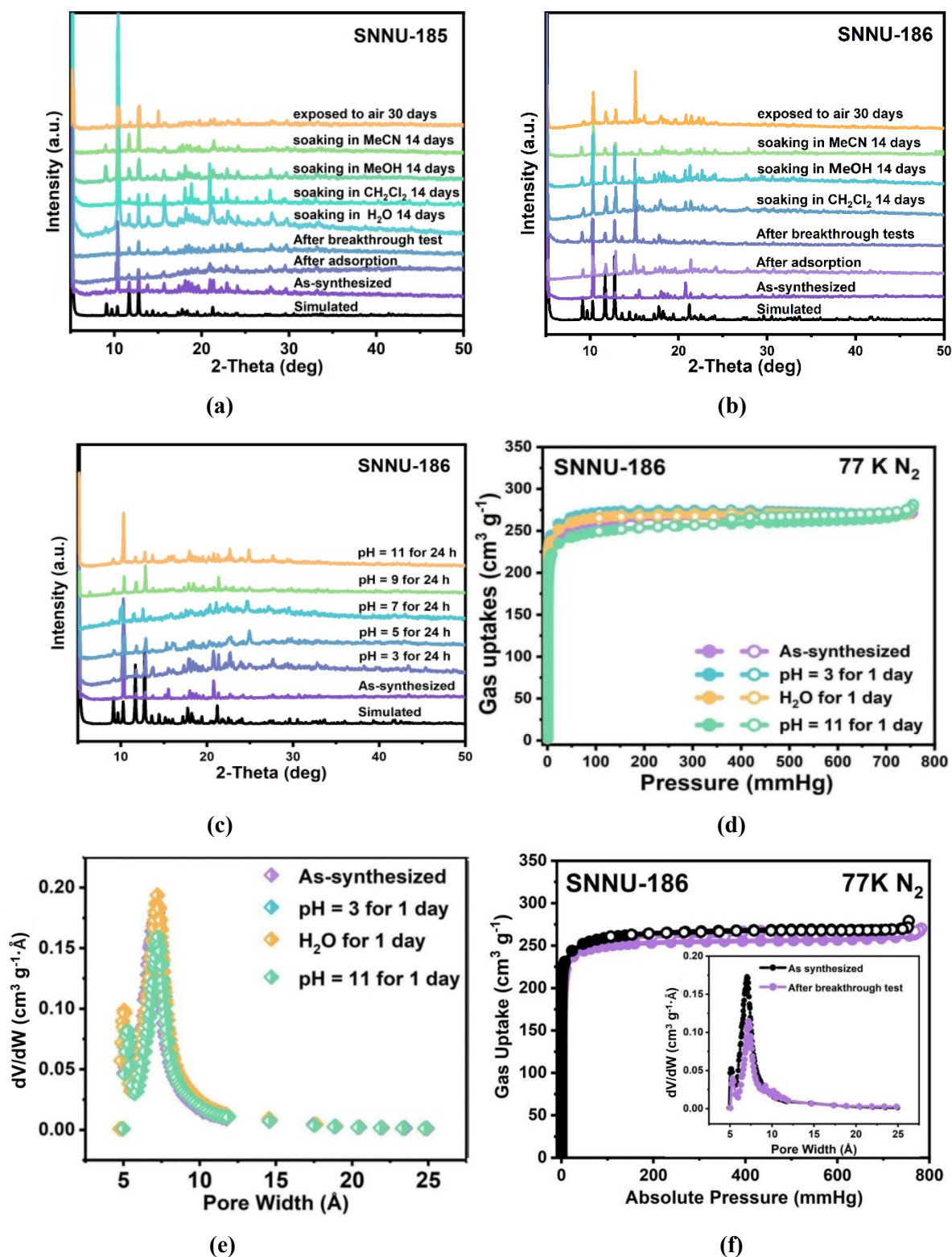
Figure S6. (a), (b) and (c) PXRD patterns of SNNU-185 and SNNU-186 after treatment under different conditions. (d) 77 K N_2 adsorption-desorption isotherms of SNNU-186 after treatment under different conditions. (e) (f) Pore size distributions calculated by using the Horvath-Kawazoe method for SNNU-186 after treated under different conditions.

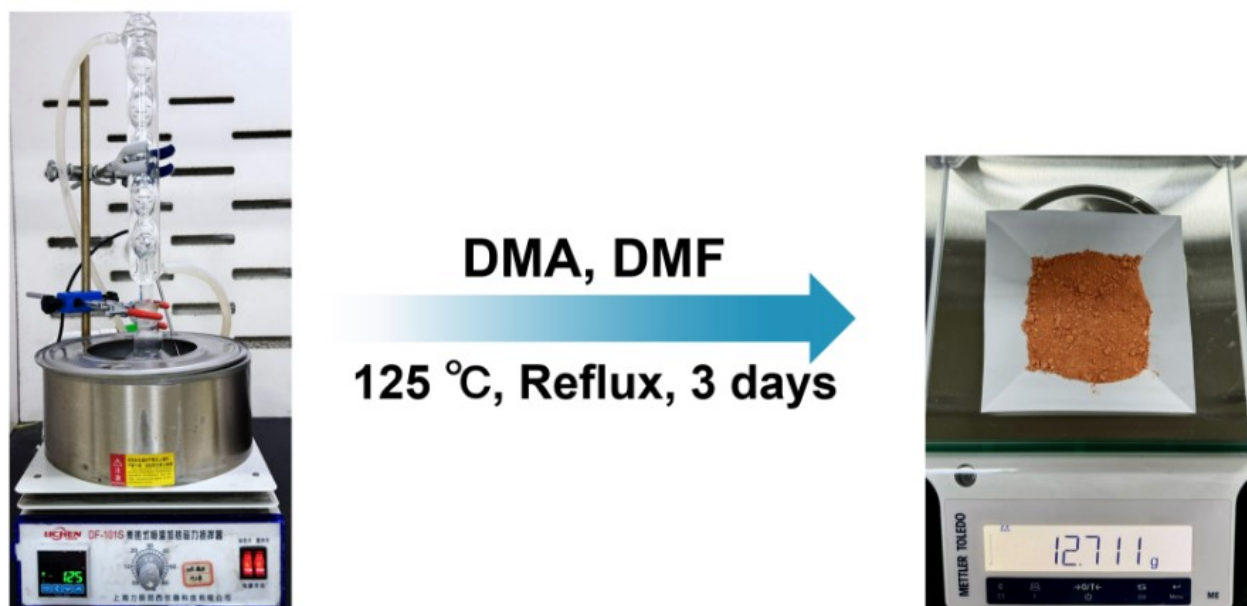**Figure S7.** Large-scaled synthesis of SNNU-186.
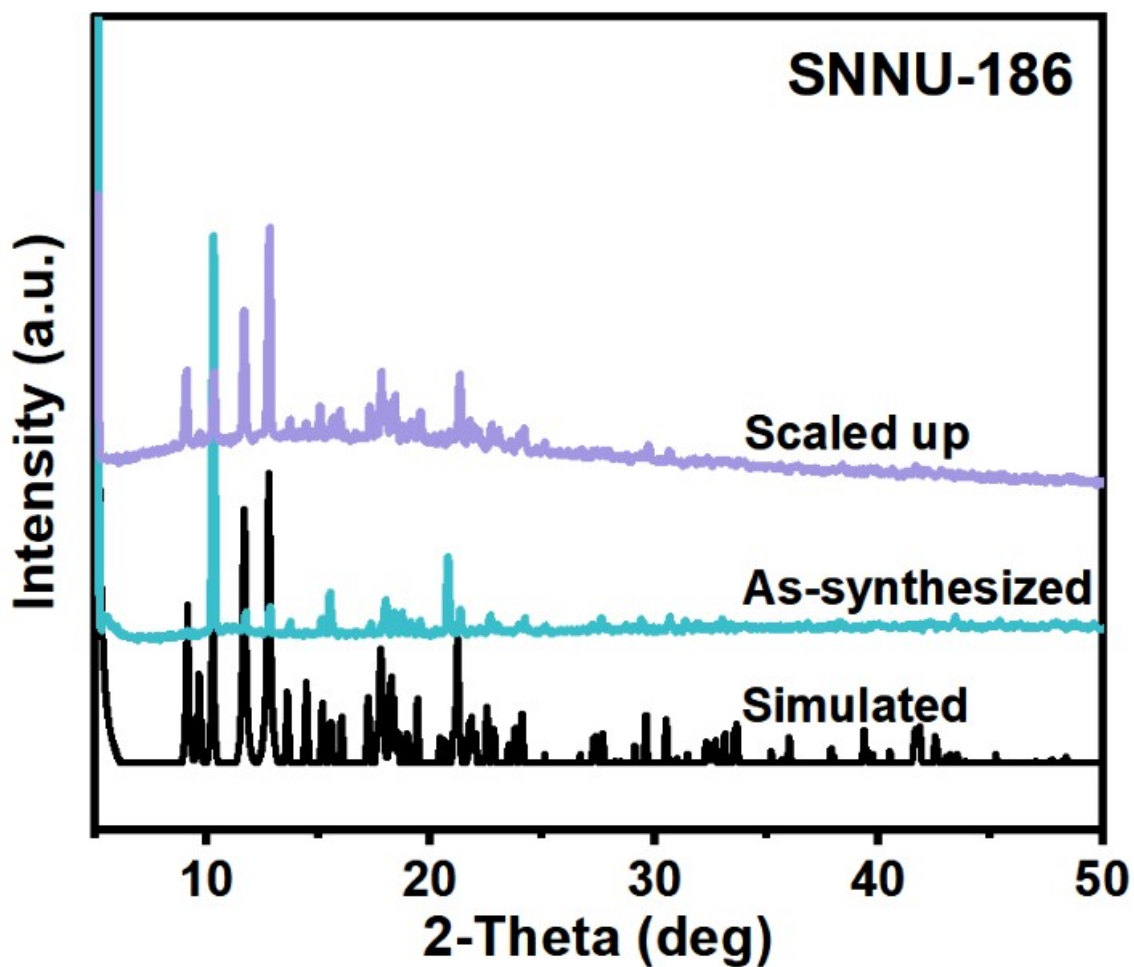
Figure S8. PXRD patterns of simulated, as-synthesized and scaled up SNNU-186.
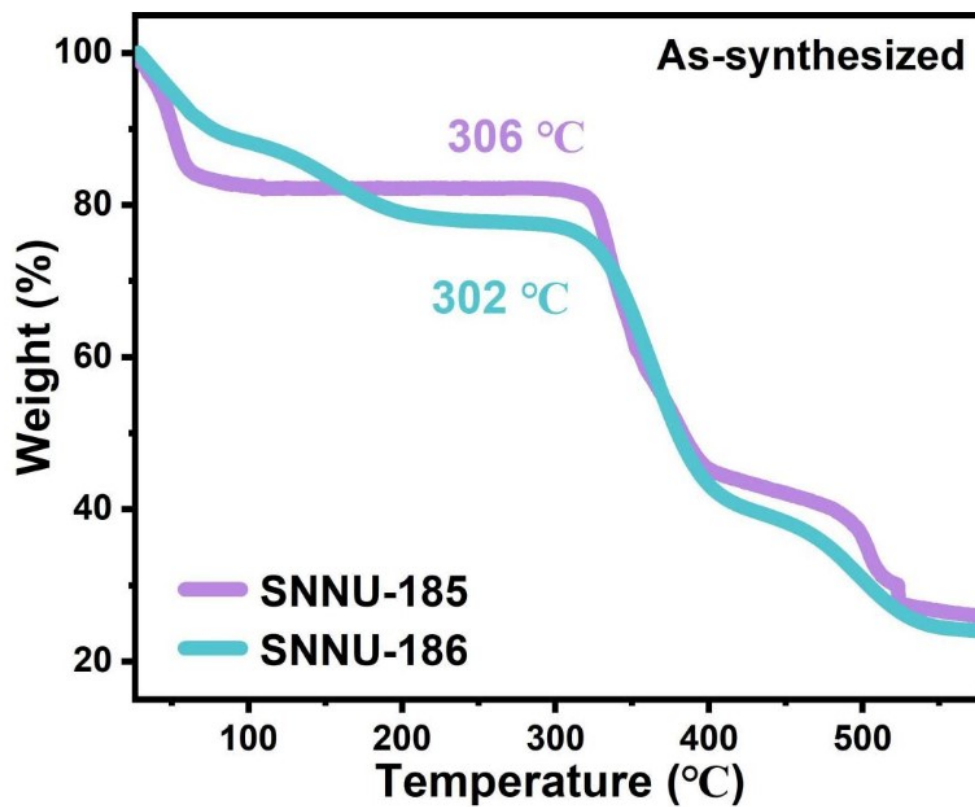
(a)
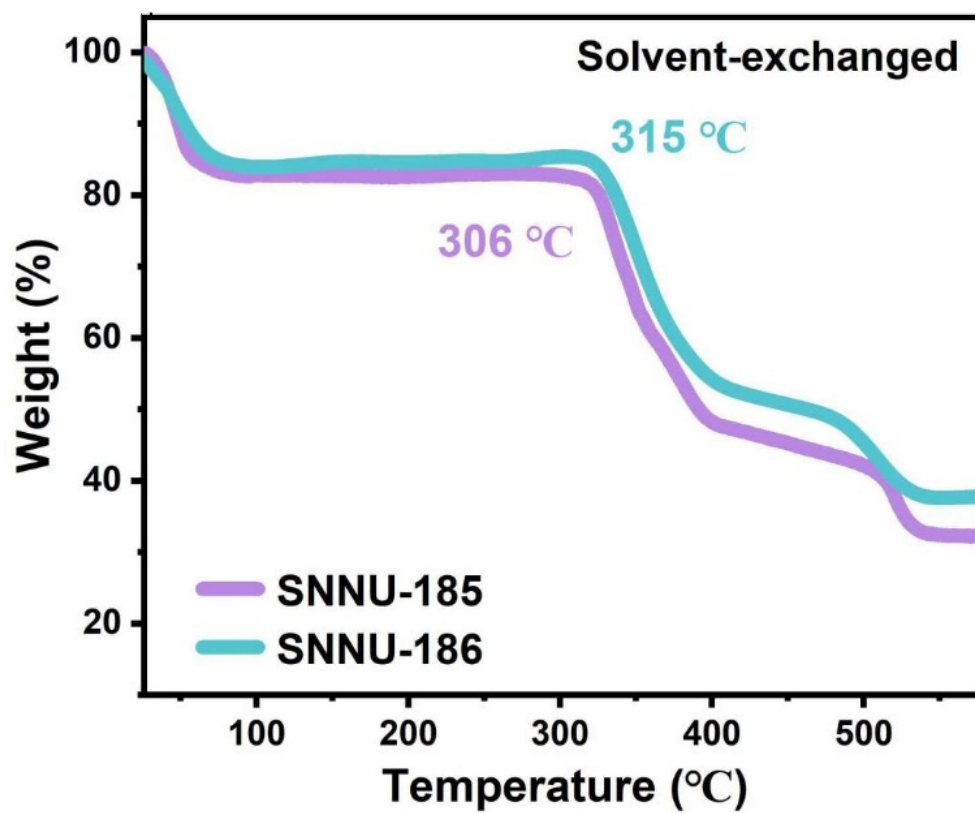
(b)

Figure S9. The TG analysis of (a) as-synthesized and (b) solvent-exchanged SNNU-185 and SNNU-186.
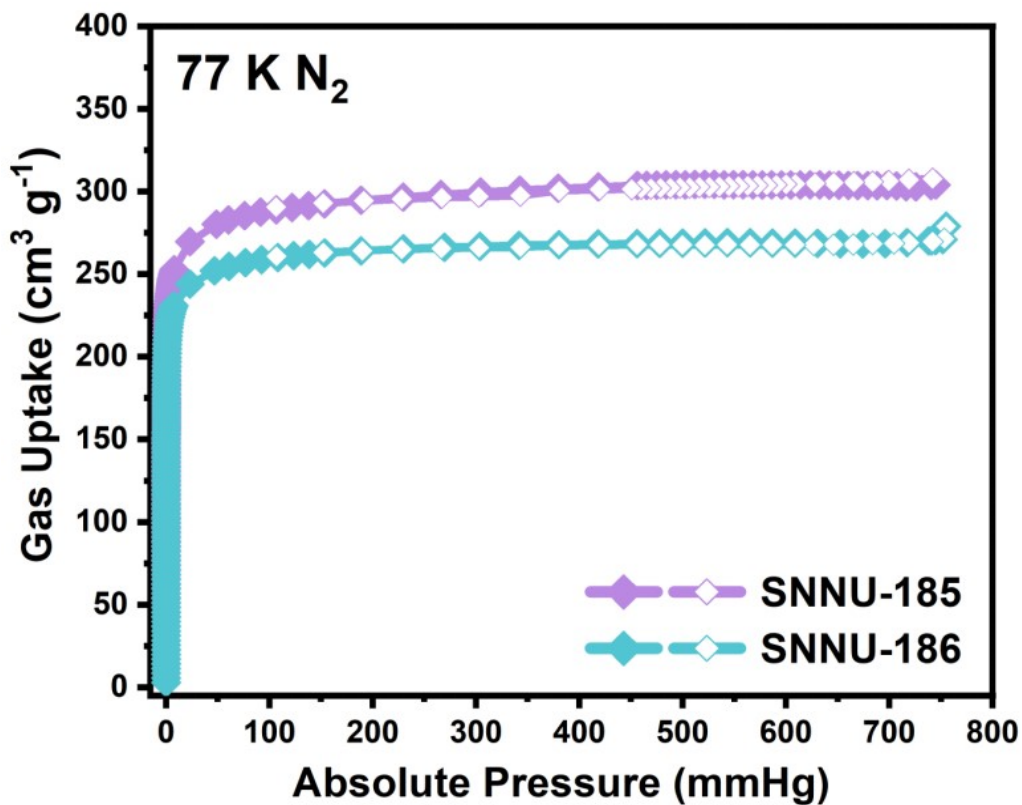
(a)
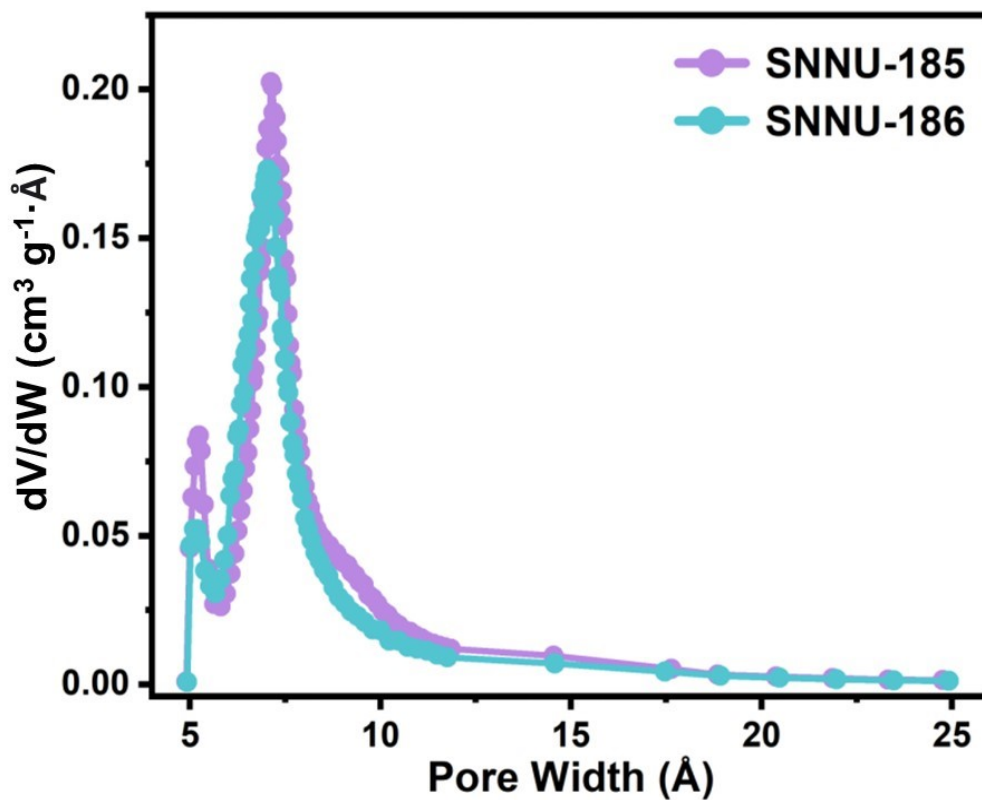
(b)

Figure S10. (a) N_2 adsorption-desorption isotherms of SNNU-185 and SNNU-186 at 77 K. (b) Pore size distributions calculated by using the Horvath-Kawazoe method for SNNU-185 and SNNU-186.
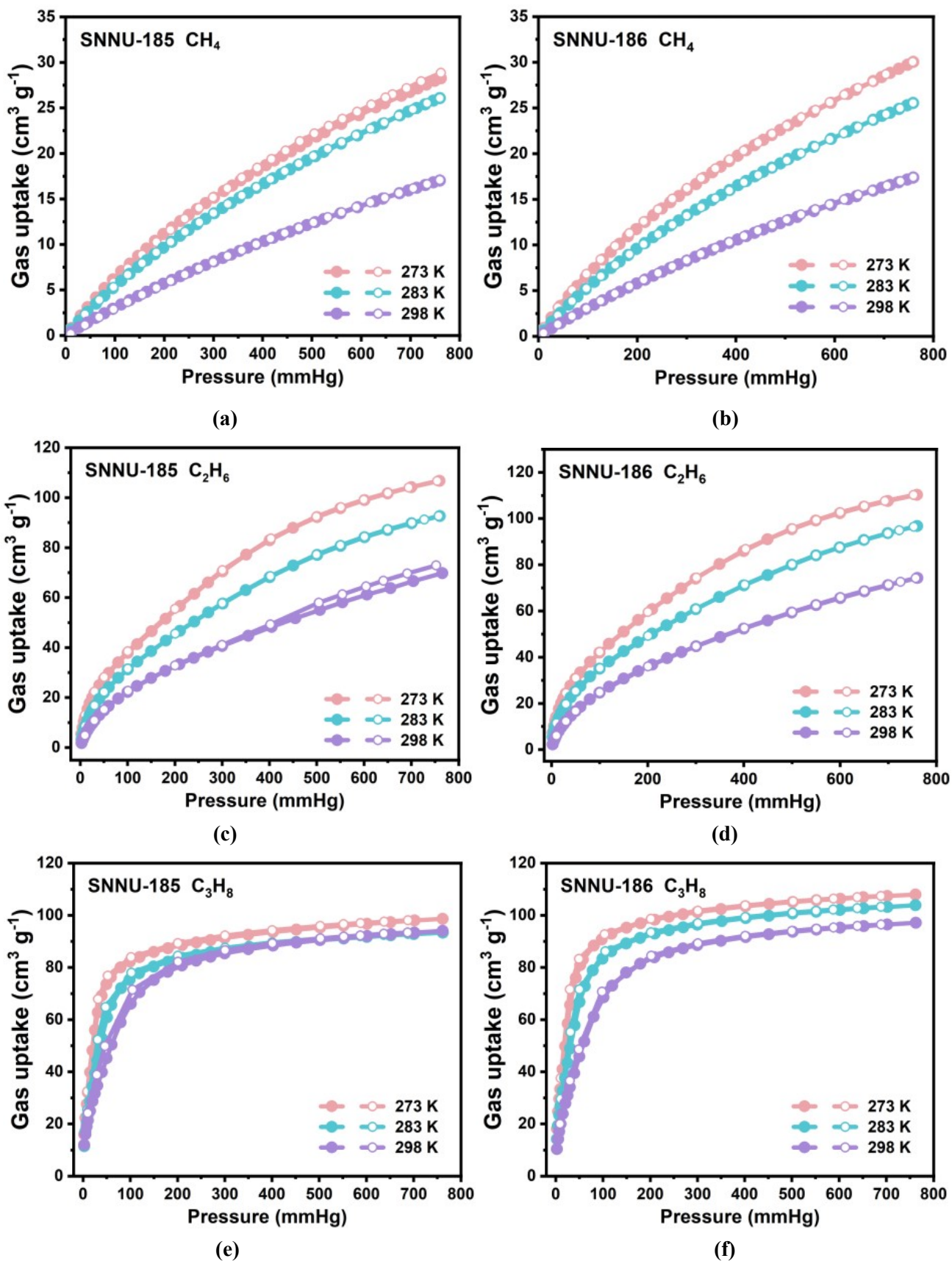
Figure S11. (a) CH$_4$, (c) C$_2$H$_6$ and (e) C$_3$H$_8$ sorption isotherms of SNNU-185 at 273/283/298 K. (b) CH$_4$, (d) C$_2$H$_6$ and (f) C$_3$H$_8$ sorption isotherms of SNNU-186 at 273/283/298 K.
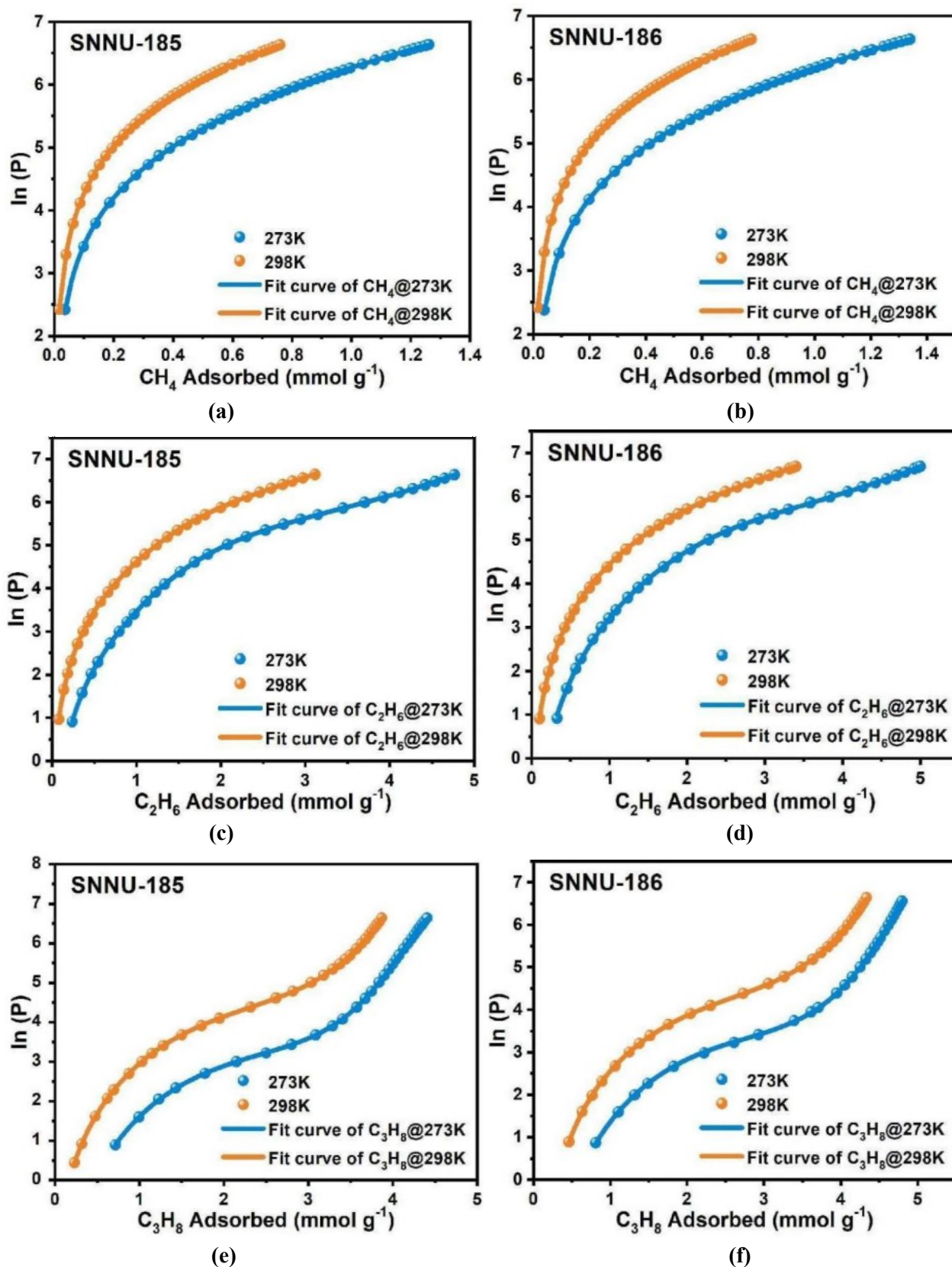
Figure S12. Fitted (a) CH_4, (c) C_2H_6 and (e) C_3H_8 adsorption isotherms of SNNU-185 measured at 273 and 298 K, and their corresponding isosteric heats of adsorption. Fitted (b) CH_4, (d) C_2H_6 and (f) C_3H_8 adsorption isotherms of SNNU-186 measured at 273 and 298 K, and their corresponding isosteric heats of adsorption.
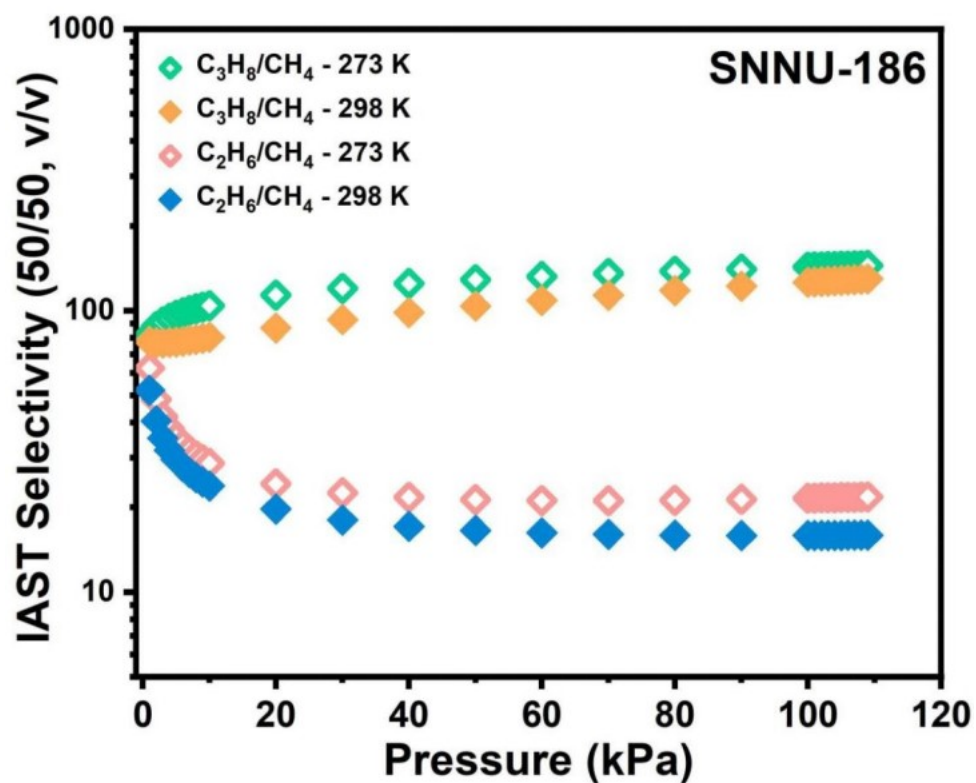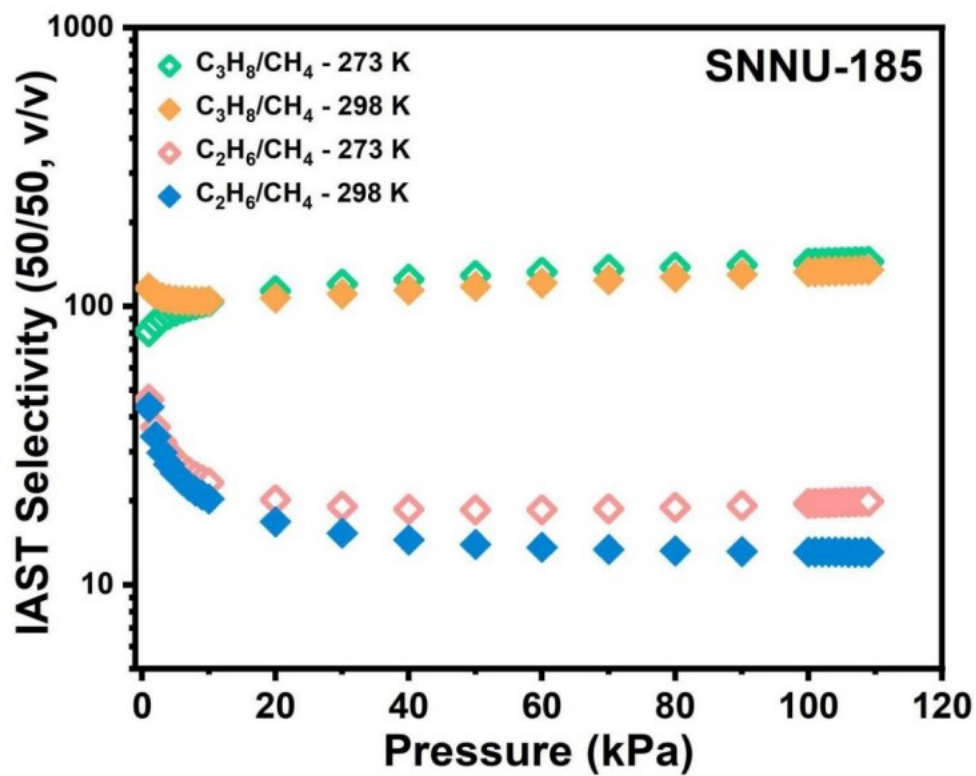
Figure S13. IAST selectivity of (a) SNNU-185 and (b) SNNU-186 for C_2H_6/CH_4 mixtures (50/50) and C_3H_8/CH_4 mixtures (50/50) at 273 and 298 K.
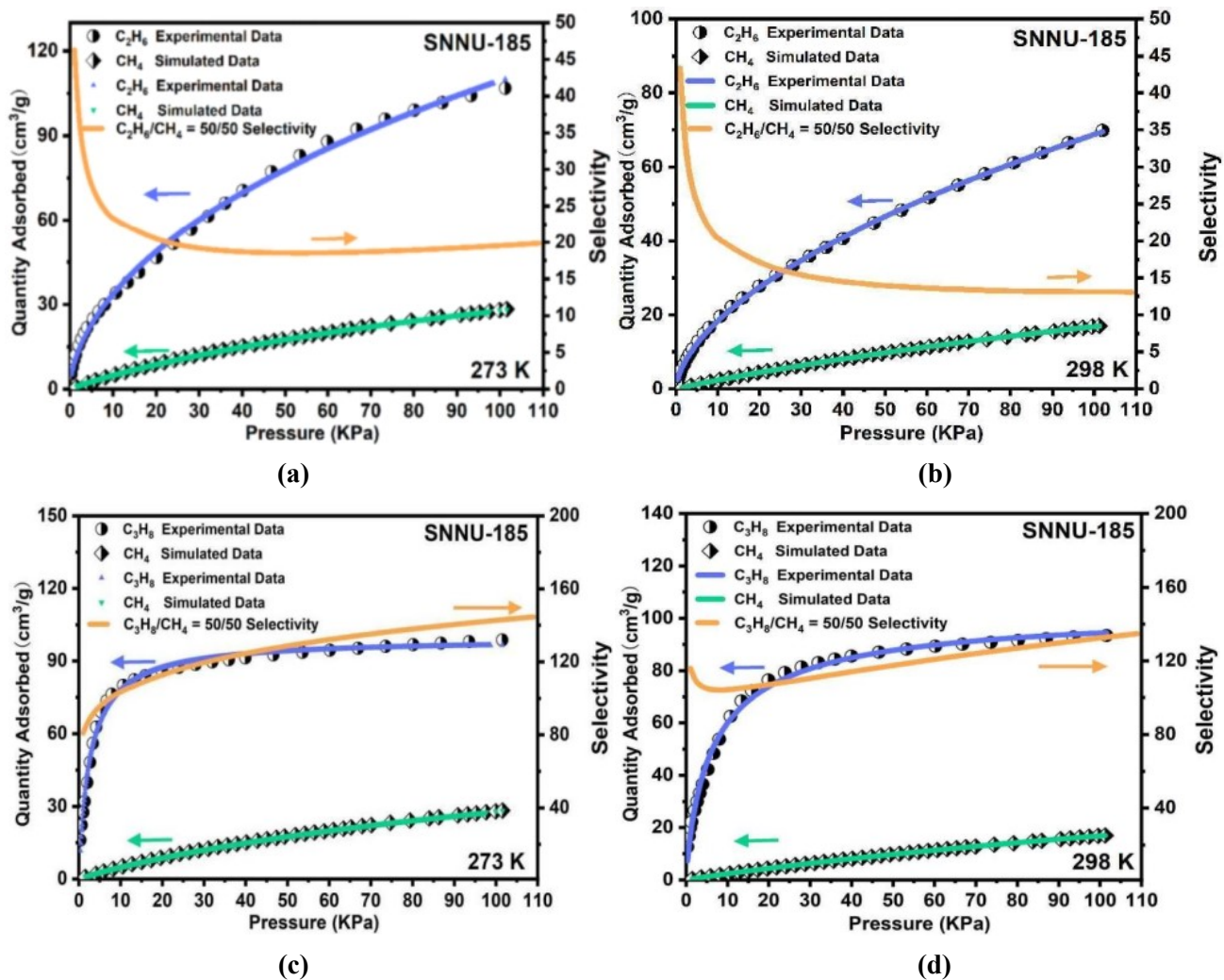
Figure S14. Comparison of experimental isotherms and simulated isotherms (left Y axis), and mixture adsorption selectivity predicted by IAST selectivity (right Y axis) for equimolar binary-mixture C_2H_6/CH_4 at (a) 273 K and (b) 298 K, and C_3H_8/CH_4 at (c) 273 K and (d) 298 K of SNNU-185.
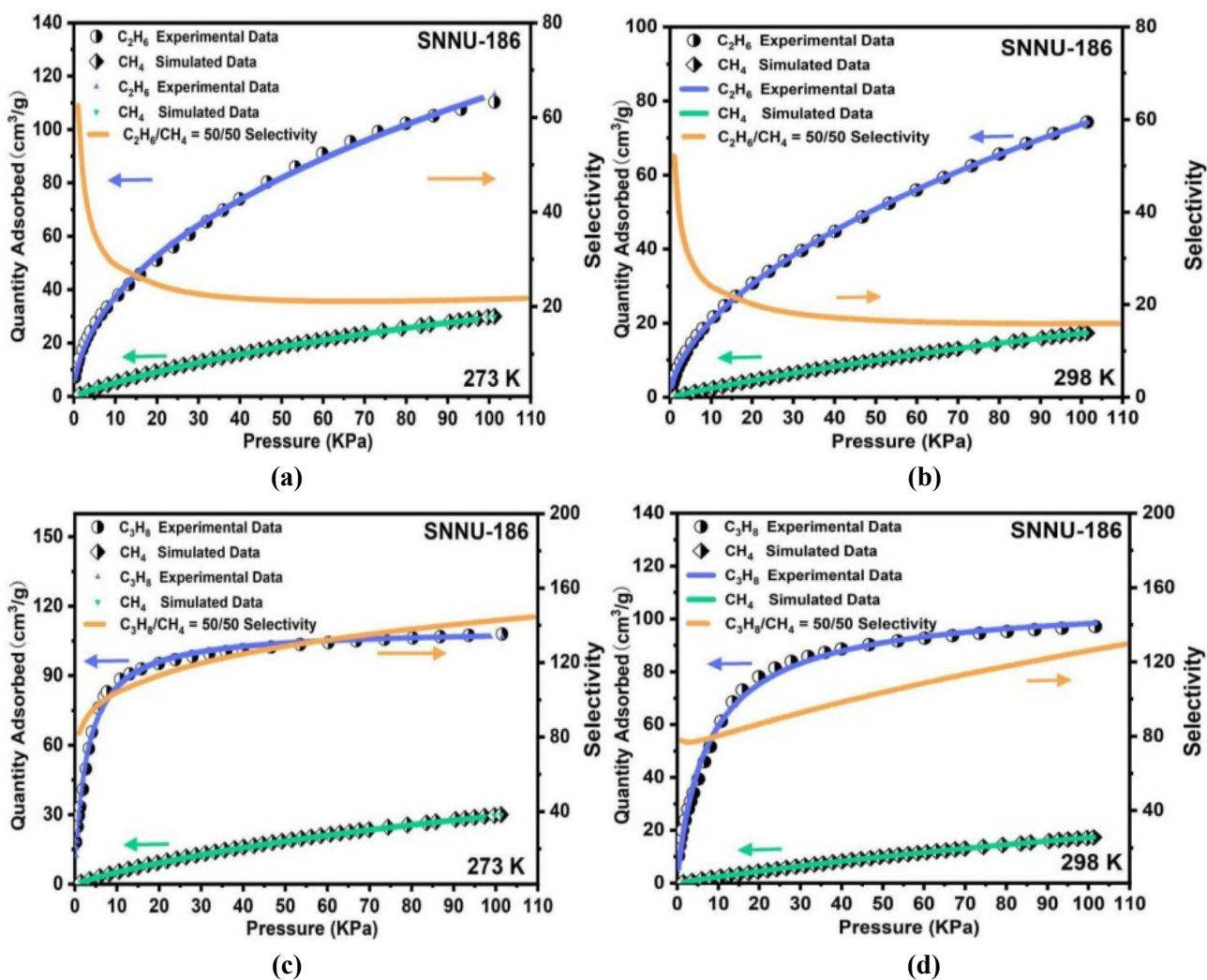
Figure S15. Comparison of experimental isotherms and simulated isotherms (left Y axis), and mixture adsorption selectivity predicted by IAST selectivity (right Y axis) for equimolar binary-mixture C_2H_6/CH_4 at (a) 273 K and (b) 298 K, and C_3H_8/CH_4 at (c) 273 K and (d) 298 K of SNNU-186.
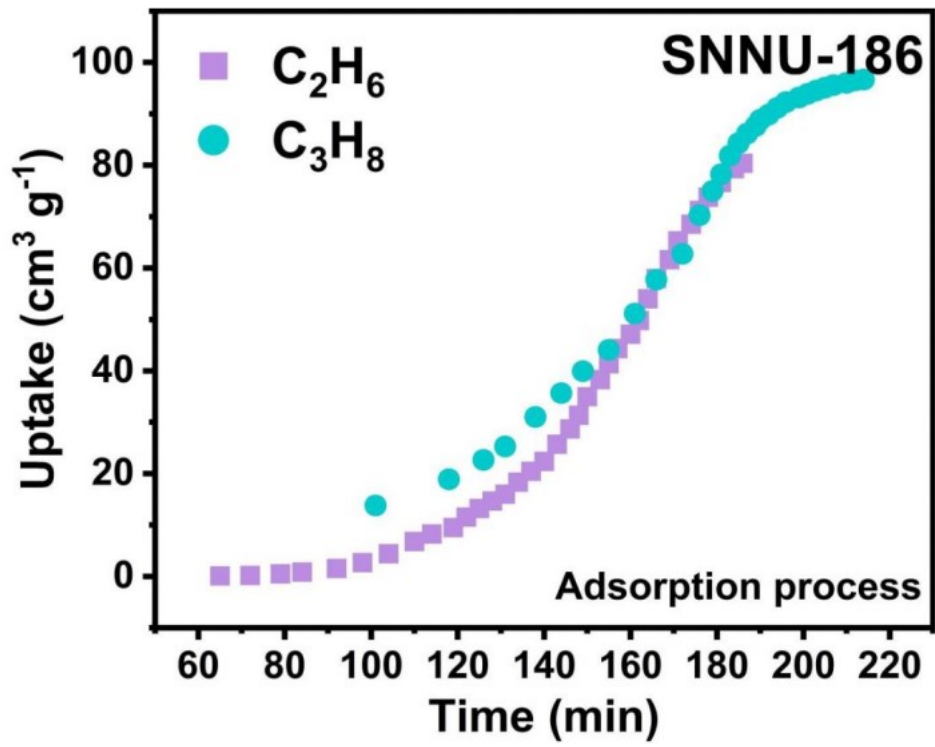
(a)
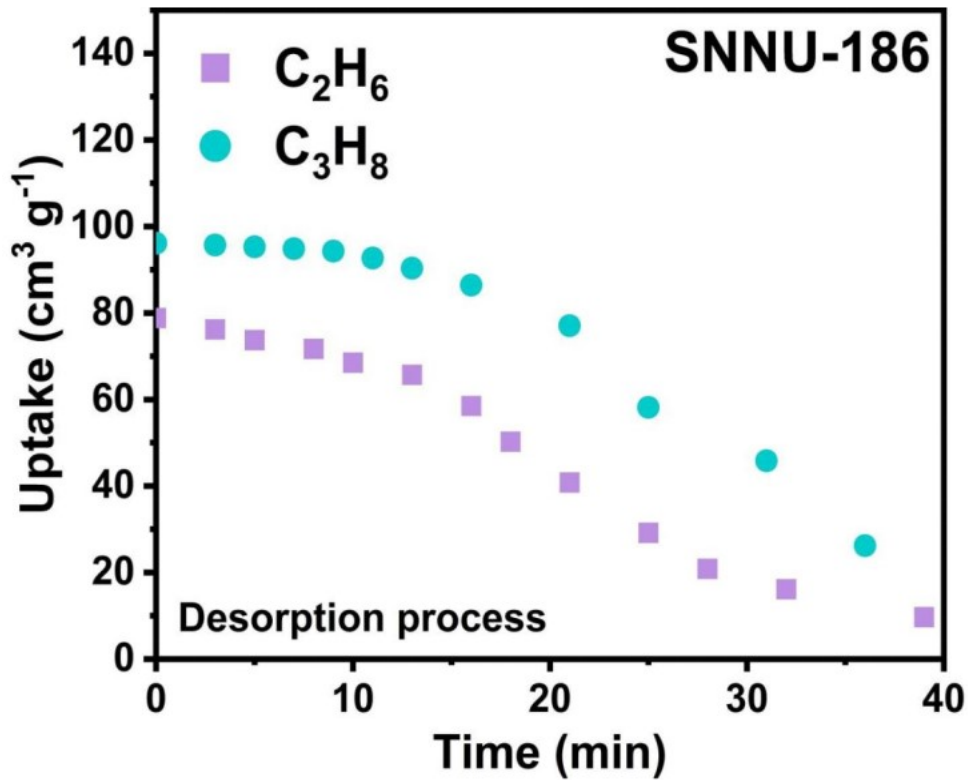
(b)

Figure S16. Time based sorption curves for C_2H_6 and C_3H_8 of SNNU-186 at 298 K.
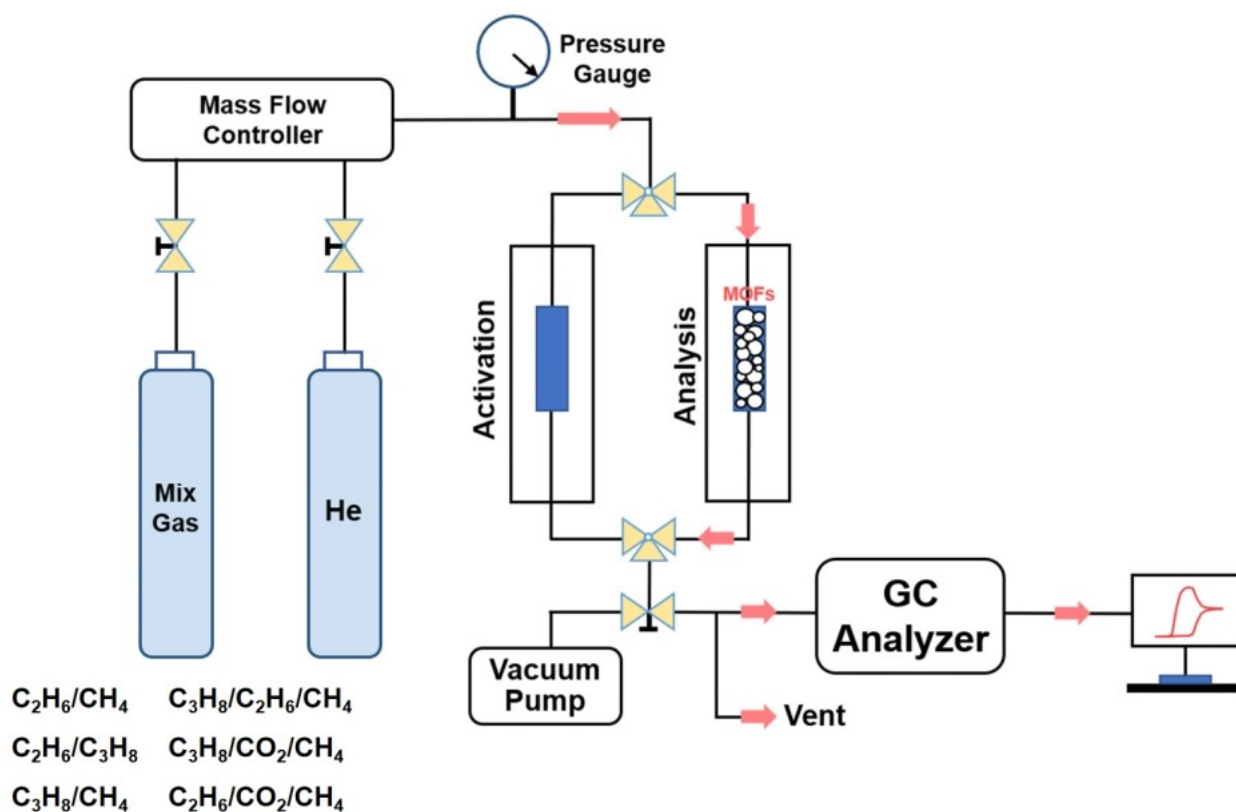
Figure S17. Schematic illustration of the apparatus for breakthrough experiments in this work.[46]
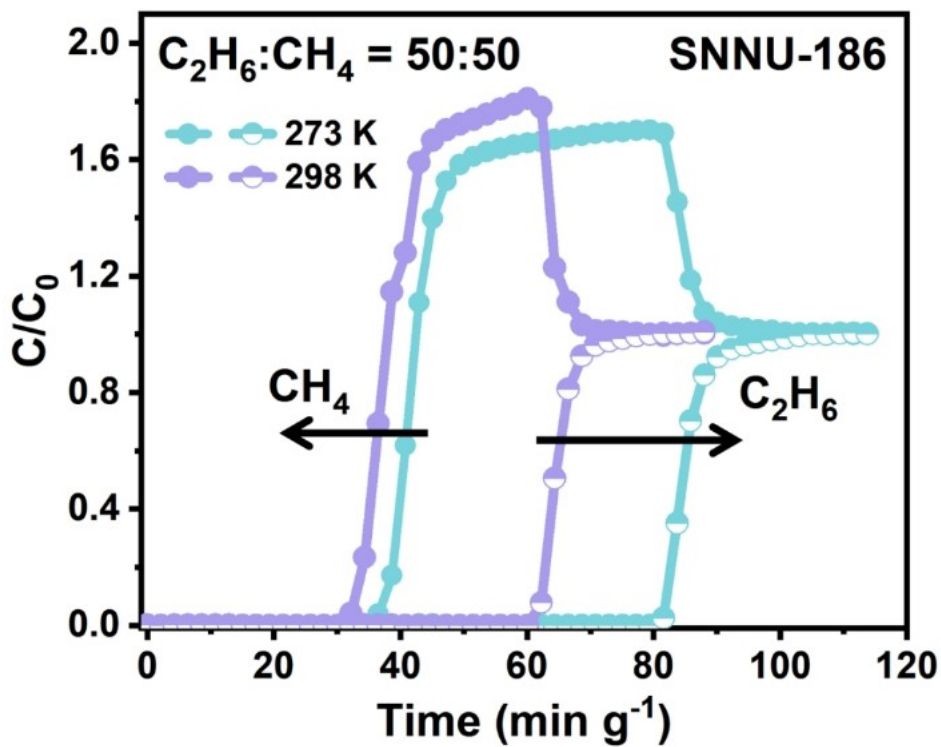
(a)
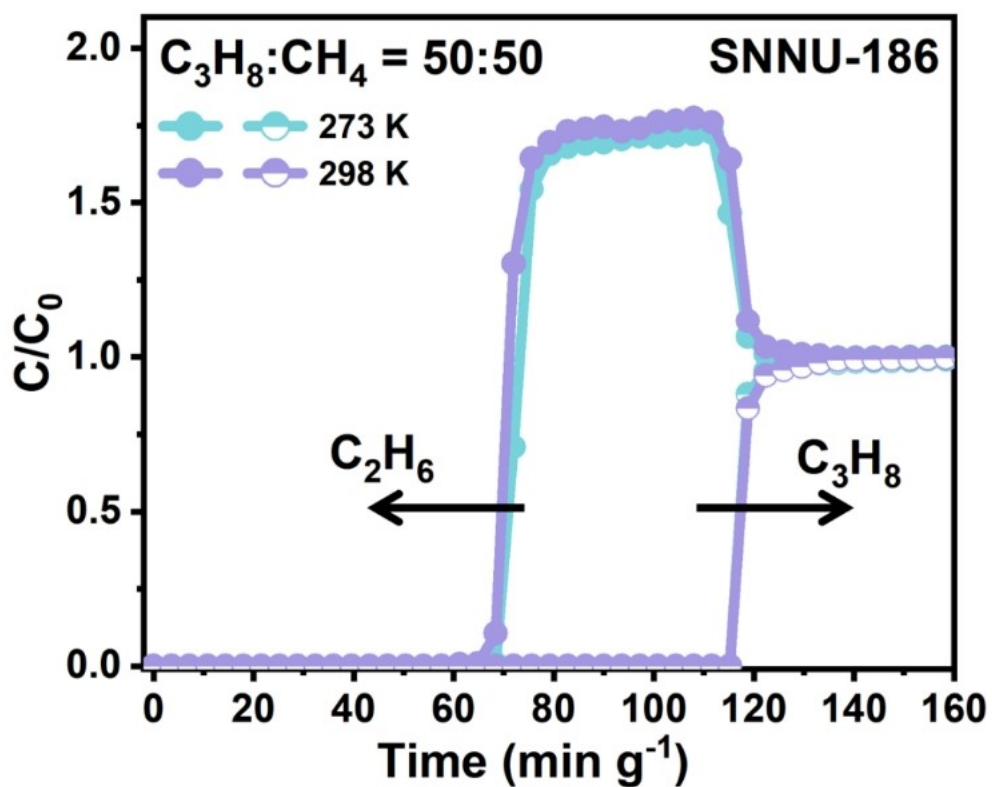
(b)

Figure S18. Experimental column breakthrough curves for (a) C_2H_6/CH_4 (50:50, v:v) and (b) C_3H_8/C_2H_6 (50:50, v:v) of SNNU-186 with a total gas flow of 2 mL min^{-1} at 273 K and 298 K.
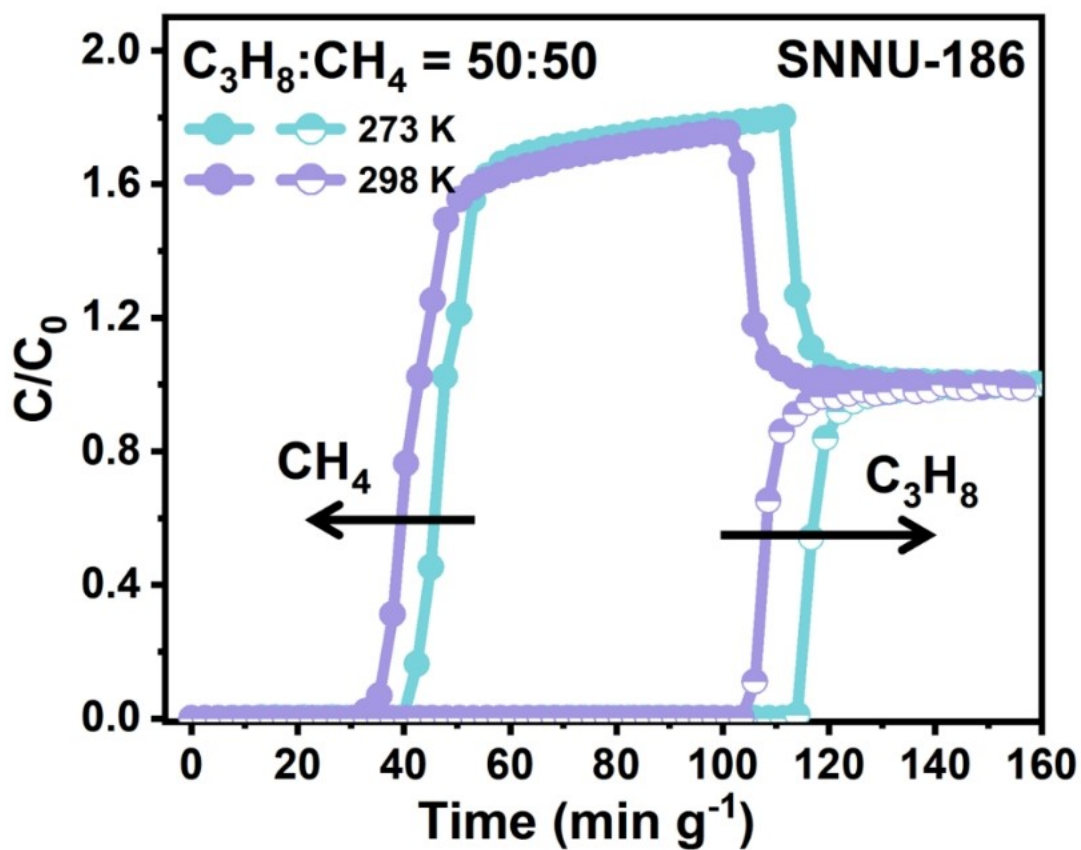
Figure S19. Experimental column breakthrough curves for CH_4/C_3H_8 (50:50, v:v) of SNNU-186 with a total gas flow of 2 mL min^{-1} at 273 K and 298 K.
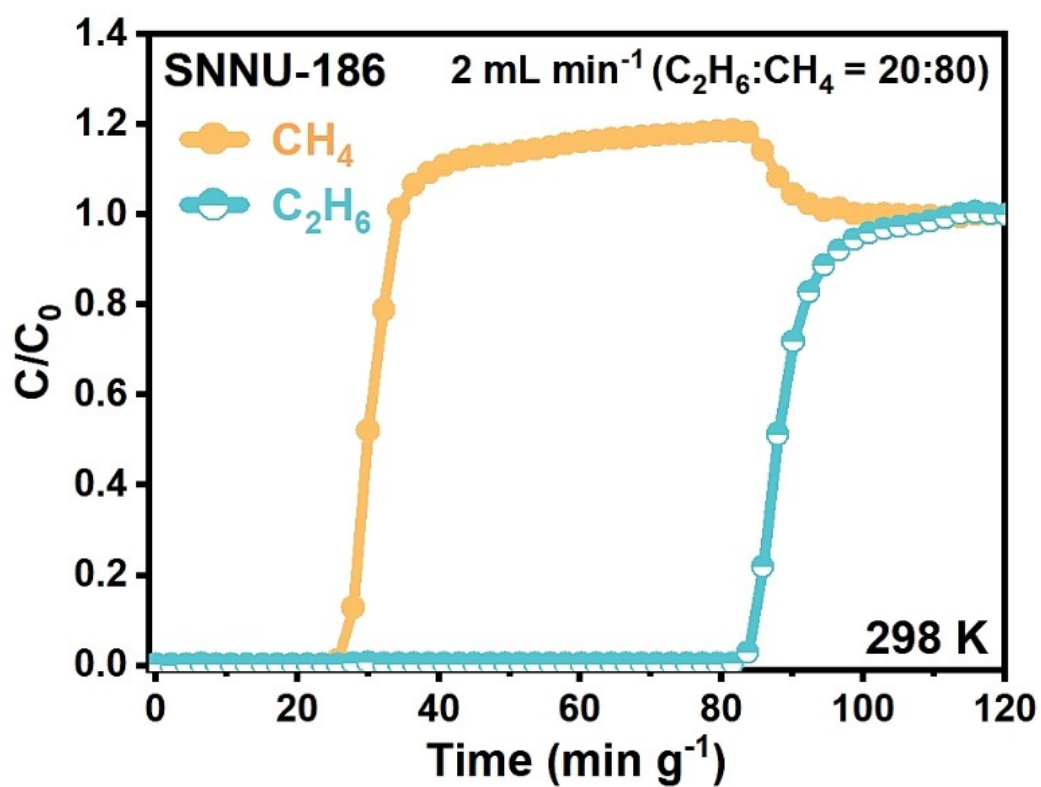
(a)
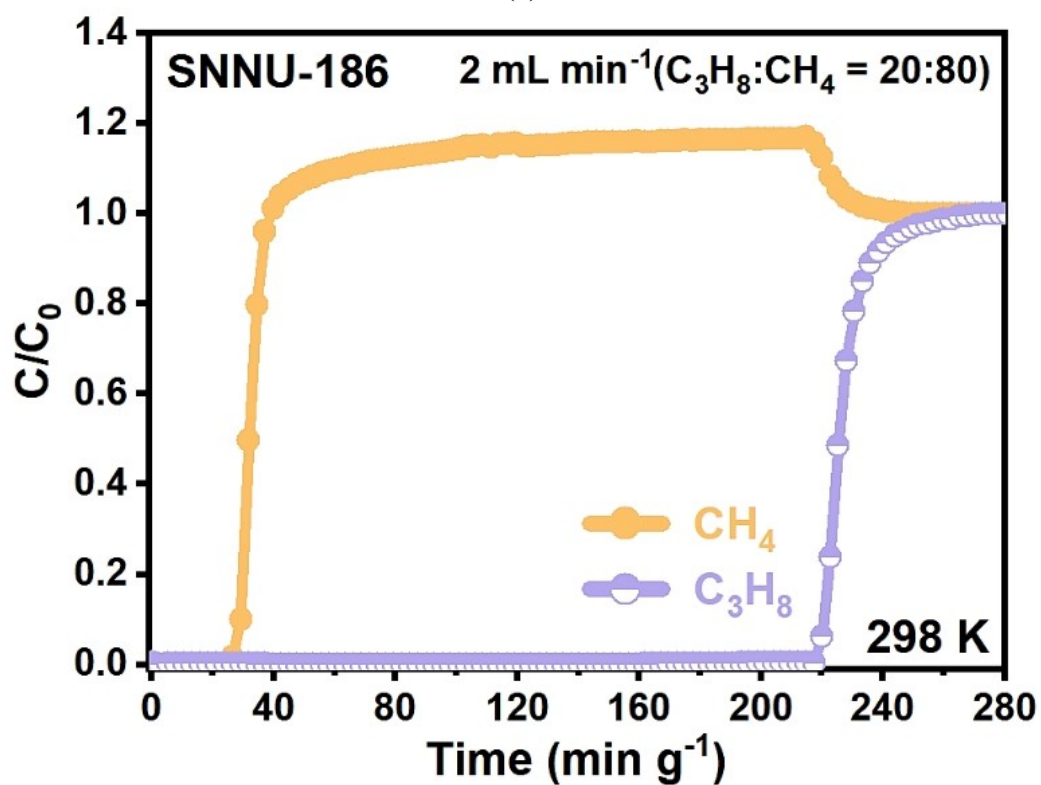
(b)

Figure S20. Experimental column breakthrough curves for (a) C_2H_6/CH_4 (20:80, v:v) and (b) $C_3H_8:CH_4$ (20:80, v:v) of SNNU-186.
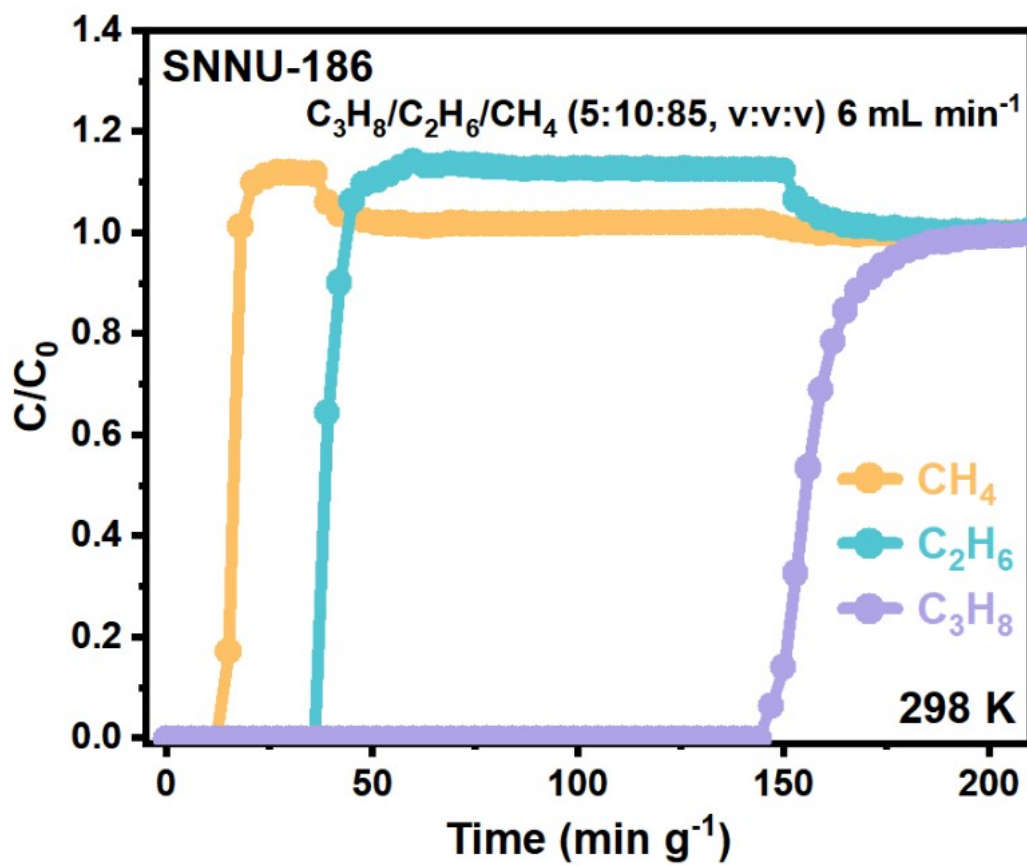
Figure S21. Experimental column breakthrough curves of SNNU-186 for $C_3H_8/C_2H_6/CH_4$ (5:10:85, v:v:v).
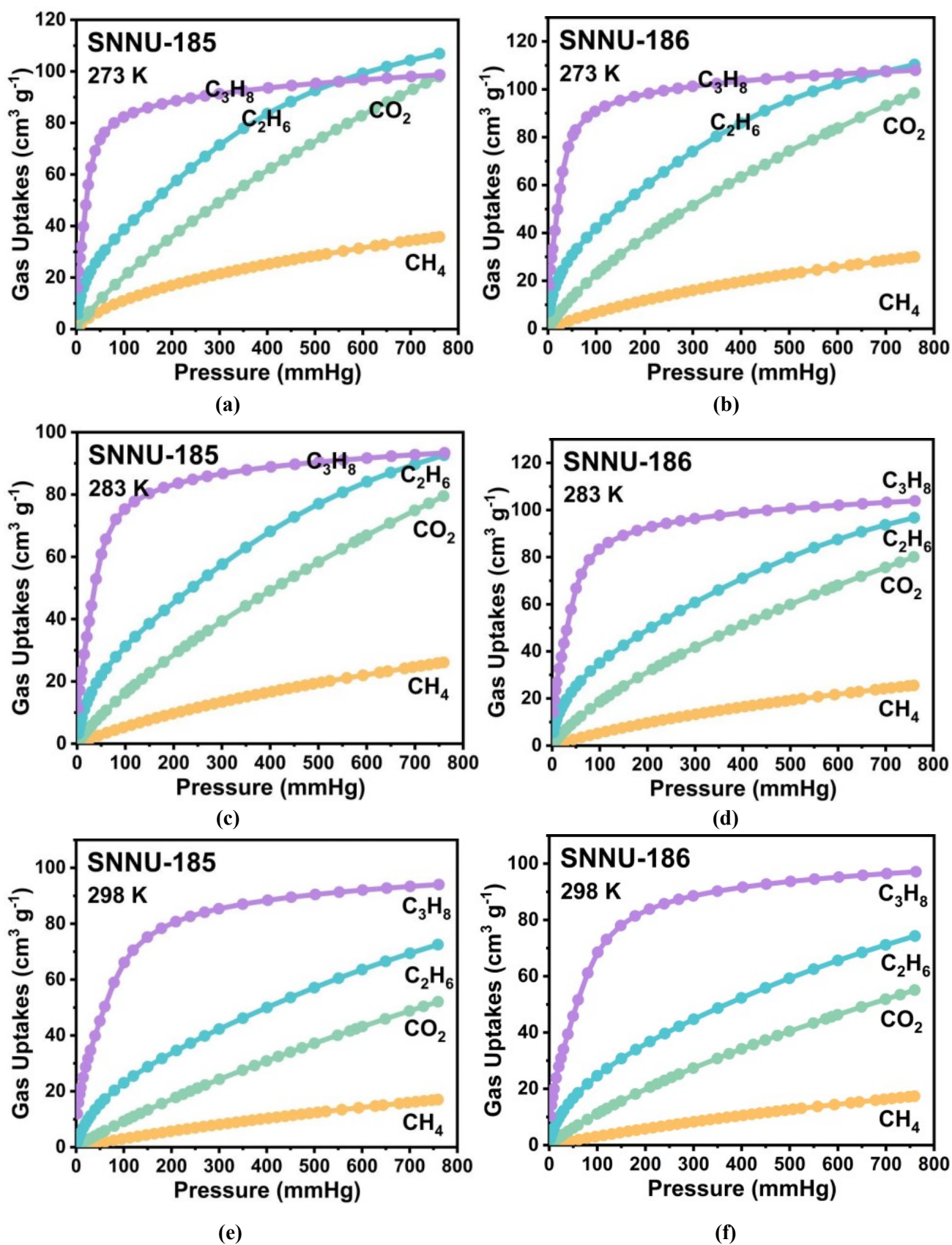
Figure S22. C$_3$H$_8$, C$_2$H$_6$, CO$_2$ and CH$_4$ sorption isotherms of SNNU-185 and SNNU-186 at 273/283/298 K.
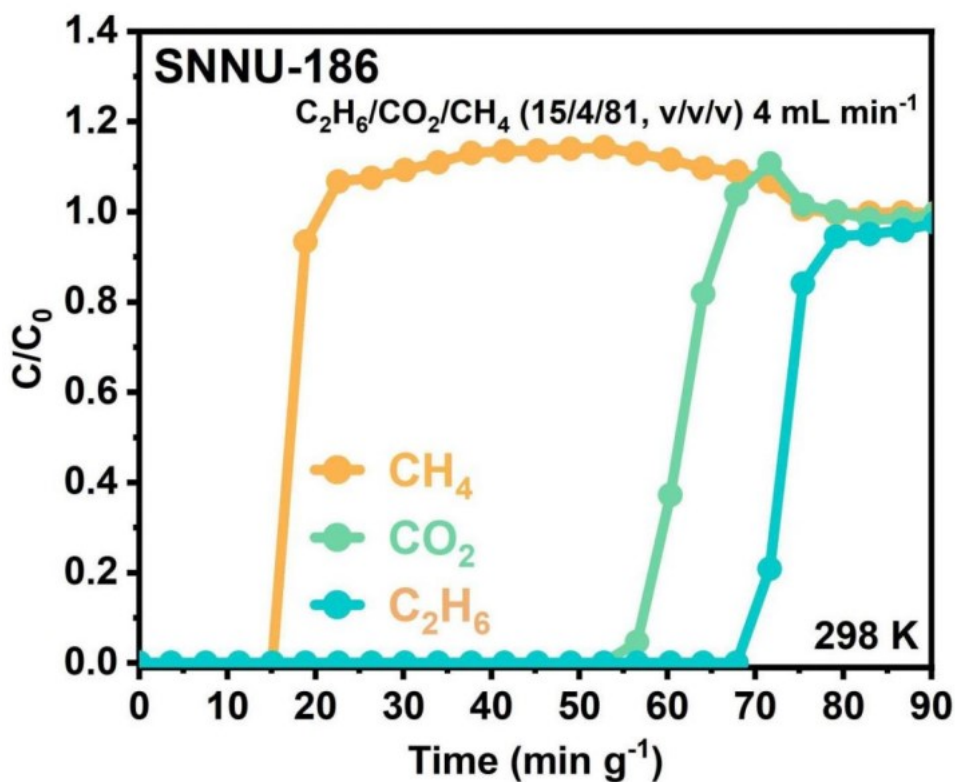
(a)
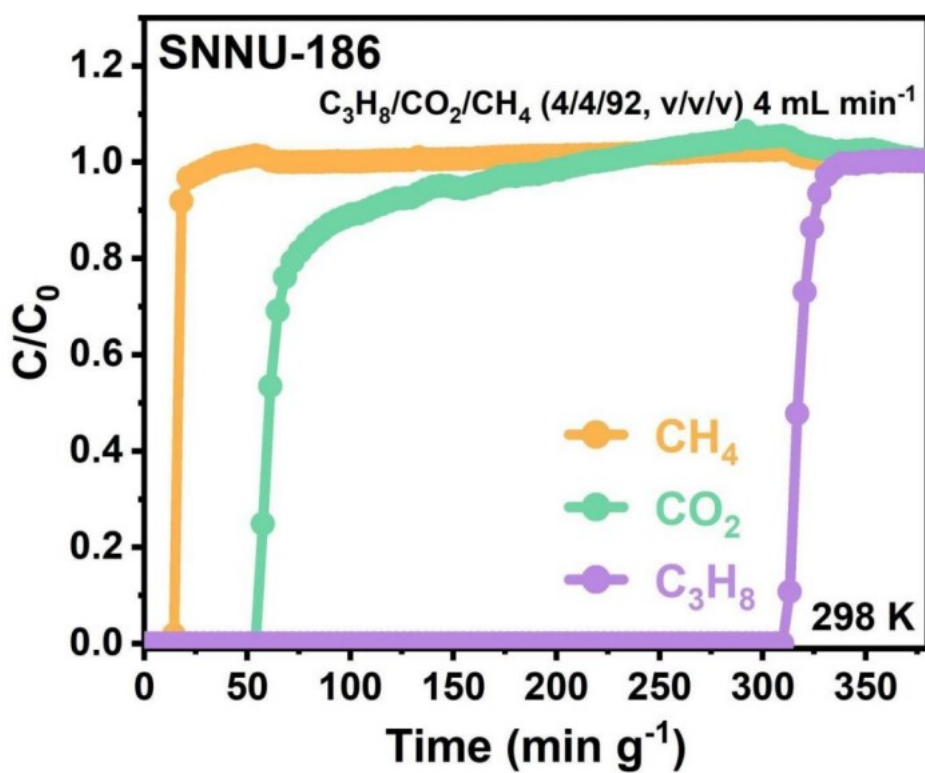
(b)

Figure S23. Experimental column breakthrough curves to evaluate the separation performance of SNNU-186 for mixed gases containing 4% CO_2 contaminants.
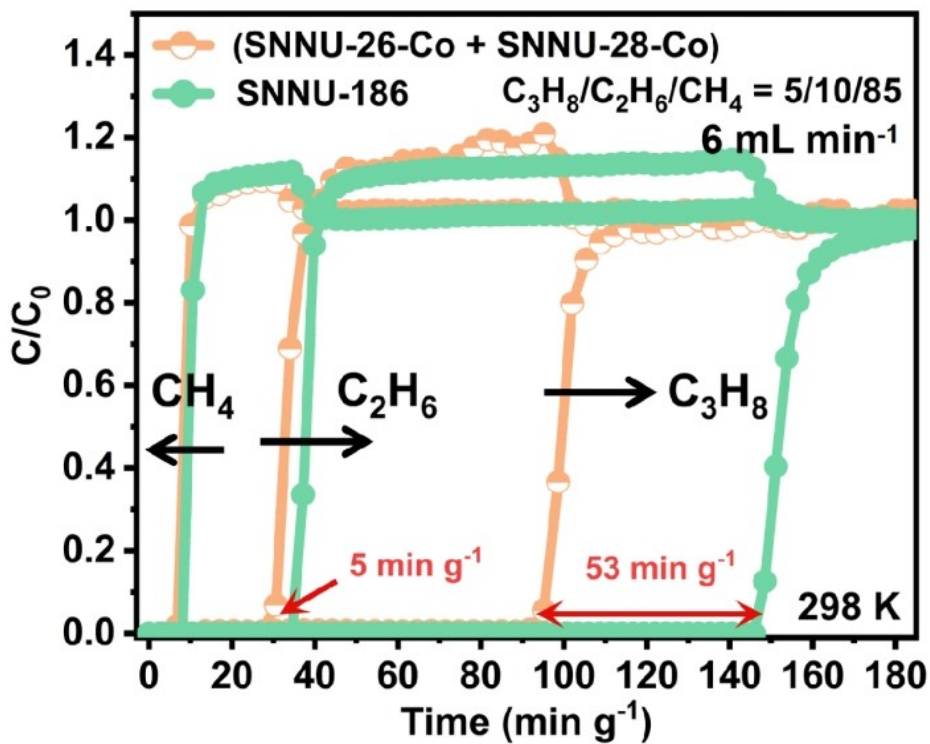
(a)
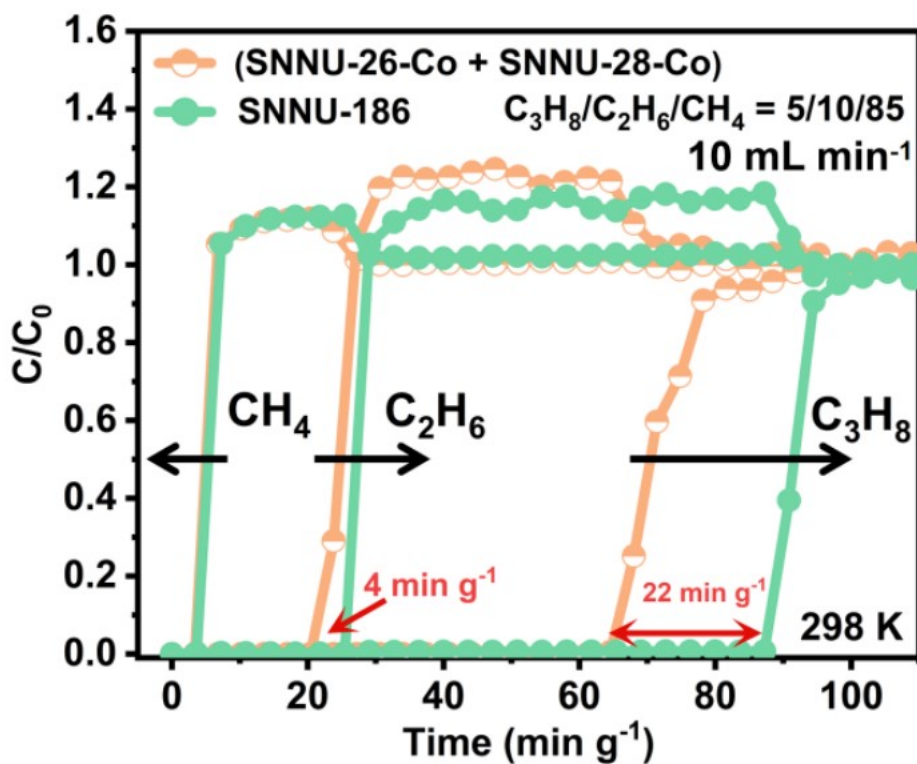
(b)

Figure S24. Under the same test conditions, comparison of experimental breakthrough curves of SNNU-186 and mixed MOFs (SNNU-26-Co+SNNU-28-Co) for $C_3H_8/C_2H_6/CH_4$ (5/10/85, v/v/v) with a total flow of (a) 6 mL min^{-1} and (b) 10 mL min^{-1} at 298 K.

(a)

(b)

(c)
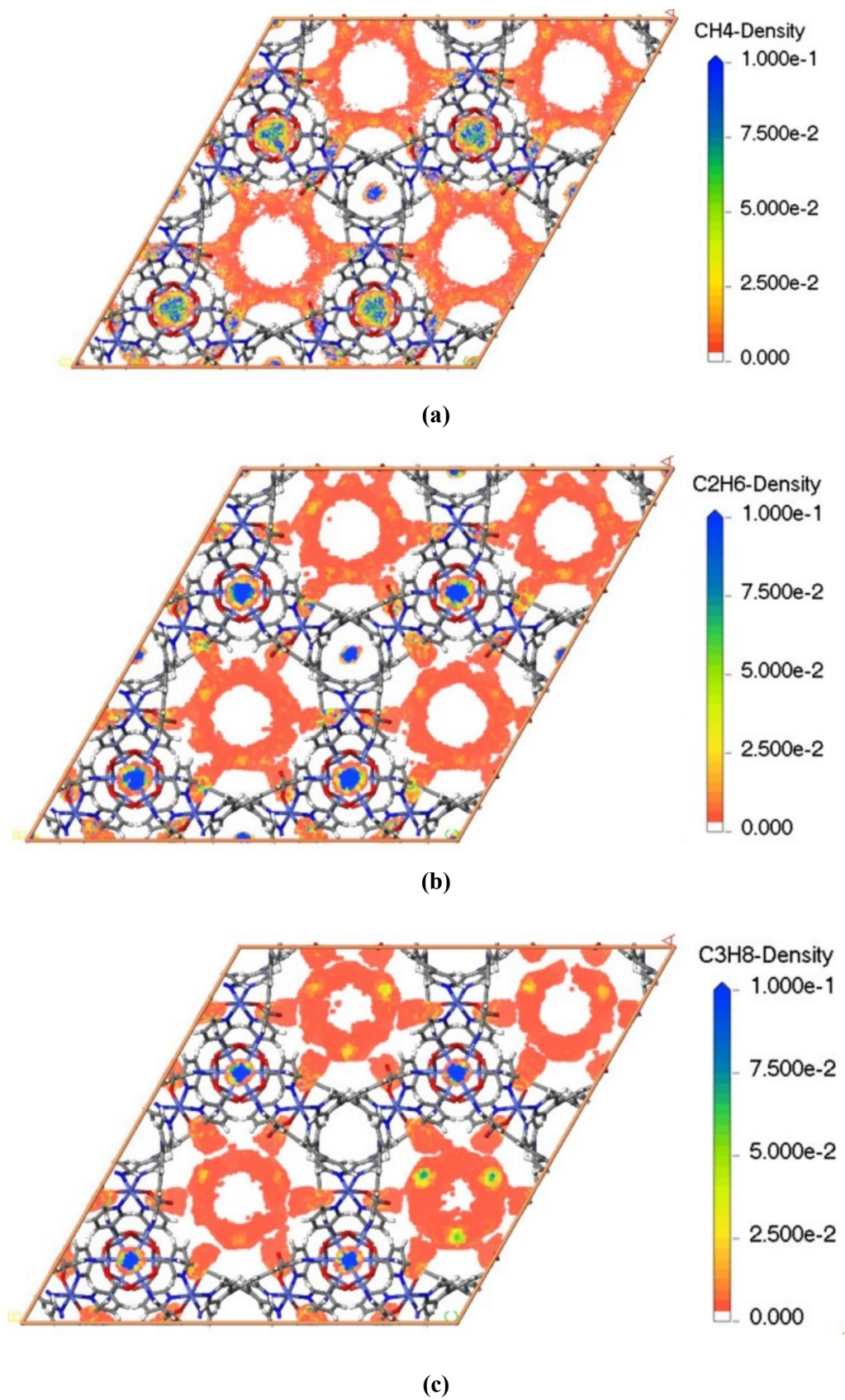
Figure S25. GCMC simulated density distributions in SNNU-186 at 298 K and 1 bar of (a) CH_4, (b) C_2H_6 and (c) C_3H_8.

Table S1. Physical properties of CH_4, C_2H_6 and C_3H_8.

Gas molecules	Molecular dimension (Å)	Kinetic diameter (Å)	Polarizability (10^{-25} cm^{-3})
CH_4	$3.76 \times 3.83 \times 3.99$	3.8	25.9
C_2H_6	$3.81 \times 4.08 \times 4.82$	4.4	44.3–44.7
C_3H_8	$4.02 \times 4.72 \times 6.20$	5.1	62.9–63.7

Table S2. Crystal data and structure refinements for SNNU-185 and SNNU-186.

Compound	SNNU-185	SNNU-186
CCDC number	2268660	2268661
Empirical formula	$C_{105}H_{63}Co_6N_{15}O_{25}$	$C_{102}H_{60}Co_6N_{18}O_{25}$
Formula weight	2288.28	2291.26
Temperature (K)	218 (13)	293 (2)
Crystal system	Hexagonal	Hexagonal
Space group	P-6c2	P-6c2
a (Å)	19.7252 (10)	19.8699 (4)
b (Å)	19.7252 (10)	19.8699 (4)
c (Å)	23.5747 (11)	23.3404 (7)
α (deg)	90	90
β (deg)	90	90
γ (deg)	120	120
Volume (Å^3)	7943.6 (9)	7980.5 (4)
Z	2	2
ρ_{calc} (g·cm^{-3})	0.957	0.954
μ (mm^{-1})	0.665	0.663
F (000)	2320.0	2320.0
2ө range for data collection (deg)	4.13 to 50.698	4.1 to 61.208
R_{int}	0.0802	0.0763
Reflections collected	30486	52454
Data/restraints	4979/6	8014/0
parameters	237	237
Goodness-of-fit on F^2	1.066	1.006
R_1, wR_2 [I > 2σ(I)]	R$_1$ = 0.0787, wR$_2$ = 0.2238	R$_1$ = 0.0673, wR$_2$ = 0.1837
R_1, wR_2 (all data)	R$_1$ = 0.0955, wR$_2$ = 0.2389	R$_1$ = 0.1213, wR$_2$ = 0.2125
Largest difference peaks (e·Å^{-3})	1.64/-0.53	0.99/-0.38

[a]$R_1 = \Sigma||F_o|-|F_c||/\Sigma|F_o|$. [b]$wR_2 = [\Sigma w(F_o^2 - F_c^2)^2/\Sigma w(F_o^2)^2]^{1/2}$

Table S3. The calculation details of Q_{st} in this work.

SNNU-185	$y = \ln(x)+(a_0+a_1 \cdot x+a_2 \cdot x^2+a_3 \cdot x^3+a_4 \cdot x^4+a_5 \cdot x^5+a_6 \cdot x^6+a_7 \cdot x^7+a_8 \cdot x^8)/c+(b_0+b_1 \cdot x+b_2 \cdot x^2)$										
	a0	a1	a2	a3	a4	a5	a6	a7	a8	Reduced Chi-Sqr	Adj. R^2
C_3H_8	-5674.91893	1934.69205	-794.47917	278.40108	-201.11293	108.51391	-34.71452	5.93378	-0.41077	8.42863E-5	0.99997
C_2H_6	-5232.29691	2329.67992	-1509.22565	1233.29357	-761.76197	275.38953	-57.38898	6.40863	-0.29732	3.60913E-5	0.99999
CH_4	-2655.66012	-188.51661	510.34605	1233.0589	-5699.04289	12034.32456	-13123.29611	7154.66389	-1542.49037	1.73107E-5	0.99998

SNNU-186	$y = \ln(x)+(a_0+a_1 \cdot x+a_2 \cdot x^2+a_3 \cdot x^3+a_4 \cdot x^4+a_5 \cdot x^5+a_6 \cdot x^6+a_7 \cdot x^7+a_8 \cdot x^8)/c+(b_0+b_1 \cdot x+b_2 \cdot x^2)$										
	a0	a1	a2	a3	a4	a5	a6	a7	a8	Reduced Chi-Sqr	Adj. R^2
C_3H_8	-5782.05258	3436.10972	-2675.84262	1792.99896	-906.95536	293.92862	-58.72869	6.63344	-0.32281	1.1505E-4	0.99996
C_2H_6	-5873.83518	2643.18132	-1103.30661	465.4955	-168.43904	31.54115	-1.9286	-0.1916	0.02383	2.30611E-4	0.99992
CH_4	-2975.07627	644.52181	-414.50362	-60.11074	1538.29931	-3485.0088	3573.85923	-1771.93965	343.97327	2.27288E-6	1

Table S4. Summary of BET surface areas, pore volumes, and isosteric heats (Q_{st}) of MOF materials reported for $CH_4/C_2H_6/C_3H_8$ separation.

MOFs	BET surface area (m² g⁻¹)	Pore size (nm)	-Q_{st} (kJ mol⁻¹)			D Q_{st} (C_2H_6-CH_4)	Ref.
			CH₄	C₂H₆	C₃H₈		
SNNU-186	**875**	**0.52/0.71**	**24.7**	**48.8**	**48.1**	**24.1**	**This work**
SNNU-185	**886**	**0.52/0.70**	**22.1**	**43.5**	**47.2**	**21.4**	
ZUL-C2	462	0.53	23	45.0	71.0	22	[4]
Ni(TMBDC)(DABCO)₀.₅	940	0.5	14、(0.5 kPa)	36 (0.5 kPa)	59 (0.5 kPa)	22	[5]
JLU-Liu6 (OMSs)	544	~0.6, 1.2	24.9	46.6	12.3	21.7	[6]
Ni-MOF 1	1125	0.57	20.7	40.2	89.5	19.5	[7]
PAN-2F (polymers)	1199	/	18.2	36.7	41.1	18.5	[8]
PAN-2 (CF₃) (polymers)	1249	/	17.4	35.6	41.7	18.2	[8]
PAN-5F (polymers)	502	/	11.6	26.7	33.0	15.1	[8]
SBMOF-2	/	/	18.0	32.3	44.0	14.3	[9]
SNNU-Bai68	959	0.31−0.42, 0.42−0.55	20.4	33.6	38.6	13.2	[10]
Ni-BPZ	790	0.59−0.93	23	36	/	13	[11]
PAN-5H (polymers)	793	/	16.2	28.7	35.7	12.5	[8]
MIL-142A	1424	0.7, 1.0	13.7	25.5	26.6	11.8	[12]
MIL-101-Fe	2617	1.10/1.55/3.22	14.5[1]	25.6	34.5	11.1	[13]
JLU-Liu15	762	0.6	23	34	40	11	[14]
JUC-220	828	0.53	28.9	33.9	41.6	11	[15]
FJI-C1	1726	1.1	11.4	21.7	28.9	10.3	[16]
UPC-33	934	0.43	3.6	13.9	18.39	10.3	[17]
ZUL-C1	504	0.43	23	33.0	54.0	10	[4]
BSF-2	403	/	23.5	32.8	39.7	9.3	[18]
MOF-160	1188	0.5−0.7	19	28	35	9	[19]
MIL-101-Fe-NH₂	2648	1.10/1.68/2.44/3.10	16.4[1]	24.6	28.3	8.2	[13]
Zn-BPZ-SA	925	0.64−0.84	~18.4	~26.4	~33	8	[20]

MIL-101-Cr	2961	1.05/1.69/3.22	14.2[1]	22.2	29.2	8	[13]
PCN-224	2704	1.2, 1.6	14	21	28	7	[21]
UPC-104	2592	1.12	8.8	15.1	26.5	6.3	[22]
LIFM-W2	583	~0.6	33.9	28.2	47.1	5.7	[23]
Fe-MOF-74 (OMSs)	1350	1.1	20	25	33	5	[24]
MOF-303	1220	0.5−0.7	19	24	34	5	[19]
BSF-1	535	/	23.7	28.6	33.7	4.4	[25]
SNNU-Bai69	627	0.64	27.4	30.6	43.8	3.2	[26]
RT-MIL-100(Fe)	2482	~1.4, 2.2	25	22	17	3	[27]
0.3Gly@HKUST-1 (OMSs)	1837	/	21.4	23.6	29.5	2.2	[28]
LIFM-ZZ-1	1076	1.24	24.9	26.8	34.5	1.9	[29]
JLU-Liu37	1795	0.86−1.1	17.5	19	29.2	1.5	[30]
ECUT-Th-10a	854	0.63, 1.2	26.4	27.3	33.6	0.9	[31]
Ni(4-DPDS)$_2$CrO$_4$	317	0.50	~30	41.6	65.2	11.6	[32]
UiO-66-Anth	676	0.57/1.01	/	28.9	35.1	/	[33]
LIFM-38	803	1.21	/	28.5	28.3	/	[34]
UiO-66-NaPh	881	0.55/1.14	/	28.3	37.9	/	[33]
PCP 1'	657	0.67	/	27.3	21.8	/	[35]
UiO-66	1305	0.86/1.11	/	26.8	32.7	/	[33]
DUT-52	1641	1.03/1.73	/	26.7	32.8	/	[33]
JUC-100	2040	1.4	27.1	26.1	/	/	[36]
JUC-106	1122	0.8	26.1	24.2	/	/	[36]
JUC-103	1484	1.0	23.5	22.6	/	/	[36]
JLU-Liu38	1784	0.86−1.1	29	19	24	/	[30]
FIR-7a-ht	1365.8	/	/	13.2	29.1	/	[37]
BSF-3	458	0.3−0.7	/	/	/	/	[38]

Table S5. The fitting parameters for Langmuir-Freundlich (LF) isotherm model of SNNU-185 and SNNU-186 in this work.

y=q*b*x^c/(1+b*x^c)					
SNNU-185	q	b	c	Reduced Chi-Sqr	Adj. R^2
C_3H_8 (273 K)	4.42995	0.39664	0.97161	0.0079	0.99388
C_3H_8 (298 K)	4.65765	0.19273	0.84636	0.01085	0.99309
C_2H_6 (273 K)	33.32287	0.01319	0.5572	0.0051	0.99775
C_2H_6 (298 K)	42.08398	0.00501	0.59799	2.89212E-4	0.99969
CH_4 (273 K)	3.80952	0.00804	0.89085	8.80072E-6	0.99993
CH_4 (298 K)	3.49178	0.00351	0.94666	5.47423E-7	0.99999

y=q*b*x^c/(1+b*x^c)					
SNNU-186	q	b	c	Reduced Chi-Sqr	Adj. R^2
C_3H_8 (273 K)	4.91807	0.37479	0.9623	0.00973	0.99940
C_3H_8 (298 K)	4.81182	0.14853	0.91885	0.01157	0.99938
C_2H_6 (273 K)	41.26234	0.01296	0.51454	0.00315	0.99986
C_2H_6 (298 K)	30.66227	0.00799	0.58867	1.61766E-4	0.99986
CH_4 (273 K)	4.22598	0.00773	0.8861	0.00973	0.99996
CH_4 (298 K)	3.27266	0.00365	0.96191	2.65427E-7	0.99999

Table S6. The comparison of CH_4 productivity, CH_4 purity, breakthrough capture capacity for C_2H_6 and C_3H_8 in $CH_4/C_2H_6/C_3H_8$ (85/10/5, v/v/v) separation at 298 K, and IAST selectivity (50/50) among reported MOFs used for ternary $C_3H_8/C_2H_6/CH_4$ separation.

MOFs	Mechanism	CH_4 productivity (mmol g^{-1})	CH_4 purity (%)	Capture capacity (mmol g^{-1})		Gas uptake (mmol g^{-1}) 298 K, 100 kPa		IAST selectivity (50/50)		Ref.
				C_2H_6	C_3H_8	C_2H_6	C_3H_8	C_2H_6/CH_4	C_3H_8/CH_4	
Ni(TMBDC)(DABCO)$_{0.5}$	Thermodynamics	12.6	/	1.78	2.98	5.81	5.54	29[c]	/	[5]
ZUL-C2	Thermodynamics	11.4	>99.9999	2.13	1.66	2.82	2.52	91	632	[4]
MOF-303	Thermodynamics	7.97	/	1.07	3.39	4.96	4.74	26[a]	/	[19]
SNNU-185	**Thermodynamics; Selective bi-nanotraps**	**6.85**	**>99.9999**	**1.23**	**2.33**	**3.12**	**4.20**	**13.1**	**126.0**	**This work**
SNNU-186		**6.10**	**>99.9999**	**0.90**	**2.15**	**3.32**	**4.33**	**15.9**	**132.5**	
SNNU-Bai68	Thermodynamics	6.10	>99.95	1.60	1.72	3.1	3.3	22.4[b]	/	[10]
Ni-MOF 1	Thermodynamics	6.1	99.5	0.78	2.10	4.56	3.56	61.0	638.9	[7]
SNNU-Bai69	Thermodynamics	5.93	/	0.69	1.21	2.0	2.5	25.3[b]	/	[26]
RT-MIL-100 (Fe)	Thermodynamics	5.58	/	0.56	1.11	2.22	6.78	6.0[c]	/	[27]
ZUL-C1	Thermodynamics	5.42	/	0.98	1.19	2.95	2.72	22	73	[4]
Cu-IPA (OMSs)	Thermodynamics	5.06	/	0.74	0.93	2.57	3.10	40	765	[38]
0.3Gly@HKUST-1	Thermodynamics	5.06	/	0.60	1.75	6.47	7.80	12.6	173.5	[28]
GNU-1a	Thermodynamics	4.28	>99.99	/	/	4.6	6.64	17.5	330.1	[40]
Zn-BPZ-SA	Thermodynamics	4.11	>99.95	0.45	1.65	2.97	2.73	10.5	40.6	[20]
MIL-142A	Thermodynamics	3.80	/	0.45	1.34	3.82	5.32	13.7	1300	[12]
BSF-2	Thermodynamics	3.79	/	0.45	0.69	1.22	1.77	53	2609	[18]
BSF-1	Thermodynamics	3.75	/	0.44	0.64	1.57	1.94	23	353	[25]
BSF-3	Thermodynamics	3.74	/	0.50	0.64	2.35	2.98	13	138	[38]
LIFM-ZZ-1	Thermodynamics	3.1	/	0.40	0.48	2.80	4.06	16[c]	/	[29]
MIL-101-Cr	Thermodynamics	2.43	/	0.25	0.60	1.59	3.35	22.5	84.3	[13]
UiO-66-NaPh	Thermodynamics	2.25	>99.1	0.18	0.77	1.24	1.39	32	741	[33]
DUT-52	Thermodynamics	2.08	>96.2	0.28	0.63	1.89	2.21	/	48	[33]
MIL-101-Fe	Thermodynamics	1.82	/	0.29	0.49	1.25	3.29	15.4	24.9	[13]
UiO-66	Thermodynamics	1.65	>99.5	0.17	0.74	1.67	1.7	8	65	[33]
MIL-101-Fe-NH$_2$	Thermodynamics	1.28	/	0.24	0.41	1.35	3.32	11.6	42.5	[13]
LIFM-W2	Thermodynamics	1.02	/	0.16	0.48	1.27	2.15	19[c]	/	[23]
ECUT-Th-10a	Thermodynamics	0.59	/	0.59	1.41	1.72	2.89	/	54.4	[31]
UiO-66-Anth	Thermodynamics	0.17	>96.0	0.15	0.29	0.70	0.90	32	535	[33]

a: 5/85 C_2H_6/CH_4 IAST selectivity;

b: 10/90 C_2H_6/CH_4 IAST selectivity;

c :10/85 C_2H_6/CH_4 IAST selectivity.

Table S7. The structure comparison of SNNU-186 with SNNU-26-Co and SNNU-28-Co.

MOFs	Metal cluster	Linker 1	Linker 2	OMSs	Pore size	Chemical environment
SNNU-186	Co_3-cluster	2,5-PDC	TPP	No	~5 Å + ~7 Å	Aromatic rings, N sites
SNNU-26-Co	Co_3-cluster	BDC	TPP	No	~5 Å	Aromatic rings, N sites
SNNU-28-Co	Co_3-cluster	BDC	TPP	No	~7 Å	Aromatic rings, N sites

References

[1]   Y.-Y. Xue, X.-Y. Bai, J. Zhang, Y. Wang, S.-N. Li, Y.-C. Jiang, M.-C. Hu, Q.-G. Zhai, *Angew. Chem. Int. Ed.* **2021**, *60*, 10122-10128.

[2]   J. Cui, Z. Zhang, L. Yang, J. Hu, A. Jin, Z. Yang, Y. Zhao, B. Meng, Y. Zhou, J. Wang, Y. Su, J. Wang, X. Cui, H. Xing, *Science* **2024**, *383*, 179-183.

[3]   Y.-Y. Xue, S.-N. Li, Y.-C. Jiang, M.-C. Hu, Q.-G. Zhai, *J. Mater. Chem. A* **2019**, *7*, 4640.

[4]   J. Zhou, T. Ke, F. Steinke, N. Stock, Z. Zhang, Z. Bao, X. He, Q. Ren, Q. Yang, *J. Am. Chem. Soc.* **2022**, *144*, 14322-14329.

[5]   Y. Wu, Z. Liu, J. Peng, X. Wang, X. Zhou, Z. Li, *ACS Appl. Mater. Interfaces* **2020**, *12*, 51499-51505.

[6]   D. Wang, T. Zhao, Y. Cao, S. Yao, G. Li, Q. Huo, Y. Liu, *Chem. Commun.* **2014**, *50*, 8648.

[7]   X.-X. Zhang, X.-Z. Guo, S.-S. Chen, H.-W. Kang, Y. Zhao, J.-X. Gao, G.-Z. Xiong, L. Hou, *Chem. Eng. J.* **2023**, *466*, 143170.

[8]   C. Wang, J. Zhang, Z. Wang, *ACS Appl. Nano Mater.* **2021**, *4*, 14060-14068.

[9]   A. M. Plonka, X. Chen, H. Wang, R. Krishna, X. Dong, D. Banerjee, W. R. Woerner, Y. Han, J. Li, J. B. Parise, *Chem. Mater.* **2016**, *28*, 1636-1646.

[10] H. Cheng, Q. Wang, L. Meng, P. Sheng, Z. Zhang, M. Ding, Y. Gao, J. Bai, *ACS Appl. Mater. Interfaces* **2021**, *13*, 40713-40723.

[11] S. Tu, L. Yu, D. Lin, Y. Chen, Y. Wu, X. Zhou, Z. Li, Q. Xia, *ACS Appl. Mater. Interfaces* **2022**, *14*, 4242-4250.

[12] Y. Yuan, H. Wu, Y. Xu, D. Lv, S. Tu, Y. Wu, Z. Li, Q. Xia, *Chem. Eng. J.* **2020**, *395*, 125057.

[13] L.-Z. Qin, X.-H. Xiong, S.-H. Wang, L. Zhang, L.-L. Meng, L. Yan, Y.-N. Fan, T.-A. Yan, D.-H. Liu, Z.-W. Wei, C.-Y. Su, *ACS Appl. Mater. Interfaces* **2022**, *14*, 45444-45450.

[14] X. Luo, L. Sun, J. Zhao, D.-S. Li, D. Wang, G. Li, Q. Huo, Y. Liu, *Cryst. Growth Des.* **2015**, *15*, 4901-4907.

[15] X. Shi, Y. Zu, X. Li, T. Zhao, H. Ren, F. Sun, *Nano Res.* **2023**, *16*, 10652-10659.

[16] Y. Huang, Z. Lin, H. Fu, F. Wang, M. Shen, X. Wang, R. Cao, *ChemSusChem* **2014**, *7*, 2647-2653.

[17] W. Fan, Y. Wang, Q. Zhang, A. Kirchon, Z. Xiao, L. Zhang, F. Dai, R. Wang, D. Sun, *Chem. Eur. J.* **2018**, *24*, 2137-2143.

[18] Y. Zhang, L. Yang, L. Wang, X. Cui, H. Xing, *J. Mater. Chem. A* **2019**, *7*, 27560.

[19] S. Xian, J. Peng, H. Pandey, T. Thonhauser, H. Wang, J. Li, *Engineering* **2023**, *23*, 56-63.

[20] G.-D. Wang, R. Krishna, Y.-Z. Li, Y.-Y. Ma, L. Hou, Y.-Y. Wang, Z. Zhu, *ACS Materials Lett.* **2023**, *5*, 1091-1099.

[21] R. Shi, D. Lv, Y. Chen, H. Wu, B. Liu, Q. Xia, Z. Li, *Sep. Purif. Technol.* **2018**, *207*, 262-268.

[22] W. Fan, X. Liu, X. Wang, Y. Li, C. Xing, Y. Wang, W. Guo, L. Zhang, D. Sun, *Inorg. Chem. Front.* **2018**, *5*, 2445.

[23] W. Wang, X.-H. Xiong, N.-X. Zhu, Z. Zeng, Z.-W. Wei, M. Pan, D. Fenske, J.-J. Jiang, C.-Y. Su, *Angew. Chem. Int. Ed.* **2022**, *61*, e202201766.

[24] E. D. Bloch, W. L. Queen, R. Krishna, J. M. Zadrozny, C. M. Brown, J. R. Long, *Science* **2012**, *335*, 6076.

[25] Y. Zhang, L. Yang, L. Wang, S. Duttwyler, H. Xing, *Angew. Chem. Int. Ed.* **2019**, *58*, 8145-8150.

[26] M. Ding, Q. Wang, H. Cheng, J. Bai, *CrystEngComm* **2022**, *24*, 2388.

[27] B. Yuan, X. Wang, X. Zhou, J. Xiao, Z. Li, *Chem. Eur. J.* **2019**, *355*, 679-686.

[28] Y. Wu, Y. Sun, J. Xiao, X. Wang, Z. Li, *ACS Sustainable Chem. Eng.* **2019**, *7*, 1557-1563.

[29] Z. Zeng, W. Wang, X. Xiong, N. Zhu, Y. Xiong, Z. Wei, J.-J. Jiang, *Inorg. Chem.* **2021**, *60*, 8456-8460.

[30] J. Li, X. Luo, N. Zhao, L. Zhang, Q. Huo, Y. Liu, *Inorg. Chem.* **2017**, *56*, 4141-4147.

[31] L. Wang, W. Zhang, J. Ding, L. Gong, R. Krishna, Y. Ran, L. Chen, F. Luo, *Nano Res.* **2023**, *16*, 3287-3293.

[32] F. Zheng, R. Chen, Z. Zhang, Q. Yang, Y. Yang, Q. Ren, Z. Bao, *Cell Rep. Phys. Sci.* **2022**, *3*, 100903.

[33] L. Zhang, X.-H. Xiong, L.-L. Meng, L.-Z. Qin, C.-X. Chen, Z.-W. Wei, C.-Y. Su, *J. Mater. Chem. A* **2023**, *11*, 12902-12909.

[34] C.-X. Chen, Z.-W. Wei, Q.-F. Qiu, Y.-Z. Fan, C.-C. Cao, H.-P. Wang, J.-J. Jiang, D. Fenske, C.-Y. Su, *Cryst. Growth Des.* **2017**, *17*, 1476-1479.

[35] D. Geng, M. Zhang, X. Hang, W. Xie, Y. Qin, Q. Li, Y. Bi, Z. Zheng, *Dalton Trans.* **2018**, *47*, 9008.

[36] J. Jia, L. Wang, F. Sun, X. Jing, Z. Bian, L. Gao, R. Krishna, G. Zhu, *Chem. Eur. J.* **2014**, *20*, 9073-9080.

[37] Y.-P. He, Y.-X. Tan, J. Zhang, *Chem. Commun.* **2013**, *49*, 11323.

[38] L. Wang, W. Sun, S. Duttwyler, Y. Zhang, *J. Solid State Chem.* **2021**, *299*, 122167.

[39] J. Luo, J. Wang, Y. Cao, S. Yao, L. Zhang, Q. Huo, Y. Liu, *Inorg. Chem. Front.* **2017**, *4*, 139.

[40] D. Lin, S. Tu, L. Yu, Y. Yuan, Y. Wu, X. Zhou, Z. Li, Q. Xia, *Ind. Eng. Chem. Res.* **2023**, *62*, 5252-5261.

[41] L. Li, X. Wang, J. Liang, Y. Huang, H. Li, Z. Lin, R. Cao, *ACS Appl. Mater. Interfaces* **2016**, *8*, 9777-9781.

[42] Y. Qiao, X. Chang, J. Zheng, M. Yi, Z. Chang, M.-H. Yu, X.-H. Bu, *Inorg. Chem.* **2021**, *60*, 2749-2755.

[43] P. Huang, C. Chen, F. Jiang, M. Wu, M. Hong, *Cryst. Growth Des.* **2019**, *19*, 3103-3108.

[44] Y. He, Z. Zhang, S. Xiang, F. R. Fronczek, R. Krishna, B. Chen, *Chem. Commun.* **2012**, *48*, 6493-6495.

[45] P. Zhang, X. Wen, L. Wang, Y. Zhong, Y. Su, Y. Zhang, J. Wang, J. Yang, Z. Zeng, S. Deng. *Chem. Eng. J.* **2020**, *381*, 122731.

[46] J.-W. Wang, S.-C. Fan, H.-P. Li, X. Bu, Y.-Y. Xue, Q.-G. Zhai, *Angew. Chem. Int. Ed.* **2023**, *62*, e202217839.